Developmental Biology 409 (2016) 39–54

Contents lists available at ScienceDirect

Developmental Biology

journal homepage: www.elsevier.com/locate/developmentalbiology

DB Letters

Dynamin-mediated endocytosis is required for tube closure, cell intercalation, and biased apical expansion during epithelial tubulogenesis in the *Drosophila* ovary

Nathaniel C. Peters, Celeste A. Berg *

University of Washington, Molecular and Cellular Biology Program and Department of Genome Sciences, Box 355065, Seattle, WA 98195-5065, United States

ARTICLE INFO

Article history:
Received 6 April 2015
Received in revised form
9 August 2015
Accepted 31 October 2015
Available online 2 November 2015

Keywords:
Dynamin
Endocytosis
Drosophila oogenesis
Epithelial tube morphogenesis
Tube closure
Cell intercalation
Apical expansion
E-Cadherin
Integrin
Adhesion remodeling

ABSTRACT

Most metazoans are able to grow beyond a few hundred cells and to support differentiated tissues because they elaborate multicellular, epithelial tubes that are indispensable for nutrient and gas exchange. To identify and characterize the cellular behaviors and molecular mechanisms required for the morphogenesis of epithelial tubes (i.e., tubulogenesis), we have turned to the *D. melanogaster* ovary. Here, epithelia surrounding the developing egg chambers first pattern, then form and extend a set of simple, paired, epithelial tubes, the dorsal appendage (DA) tubes, and they create these structures in the absence of cell division or cell death. This genetically tractable system lets us assess the relative contributions that coordinated changes in cell shape, adhesion, orientation, and migration make to basic epithelial tubulogenesis. We find that Dynamin, a conserved regulator of endocytosis and the cytoskeleton, serves a key role in DA tubulogenesis. We demonstrate that Dynamin is required for distinct aspects of DA tubulogenesis: DA-tube closure, DA-tube-cell intercalation, and biased apical-luminal cell expansion. We provide evidence that Dynamin promotes these processes by facilitating endocytosis of cell–cell and cell–matrix adhesion complexes, and we find that precise levels and sub-cellular distribution of E-Cadherin and specific Integrin subunits impact DA tubulogenesis. Thus, our studies identify novel morphogenetic roles (i.e., tube closure and biased apical expansion), and expand upon established roles (i.e., cell intercalation and adhesion remodeling), for Dynamin in tubulogenesis.

1. Introduction

Epithelial tubes perform numerous critical functions in metazoan physiology, and these functions often depend on specific tube morphologies. The fidelity of epithelial tube morphogenesis during development is therefore essential. Errors in these morphogenetic programs can result in harmful, even fatal, developmental defects, and mis-regulation is associated with metastatic cancers (Wallingford, 2005; Andrew and Ewald, 2010; Ray and Niswander, 2012; Iruela-Arispe and Beitel, 2013).

Tubulogenesis typically involves tube formation, tube elongation, and tube elaboration; each of these three events requires tight regulation of cell adhesion and cell polarity. The formation of a tube lumen from a polarized epithelium can be achieved through several mechanisms, including wrapping, which produces a tube parallel to the original epithelial sheet. At the cellular level, these tissue behaviors require apical constriction, basal nuclear positioning and, in the case of wrapping, the formation of new cell–cell adhesions to close the tube. Once formed, the elongation of the tube lumen is achieved through oriented cell shape-change, rearrangement, proliferation, recruitment, and migration. Elaboration of a tube lumen can be simple or even unnecessary, if the terminal tube morphology is also simple. Or, it can be highly complex and require intricate bifurcation, side branching, or clefting, events that can be either programmed or stochastic (Andrew and Ewald, 2010; Iruela-Arispe and Beitel, 2013). Relative to the cellular behaviors that drive tube formation, less is known about the mechanisms that regulate tube elongation and elaboration: How do epithelia achieve specific tube morphologies following tube formation, and what genes, molecules, and mechanisms are responsible for these cellular behaviors?

To address these questions we use the *Drosophila* ovary, and we study the formation of epithelial tubes involved in synthesizing the dorsal respiratory appendages (DAs) of the eggshell (reviewed by Berg, 2005). DA tubulogenesis exhibits many features that make it particularly attractive as a model for epithelial tube formation and elongation. First, this process is simple: a) each DA-tube

* Corresponding author.
E-mail address: caberg@uw.edu (C.A. Berg).

http://dx.doi.org/10.1016/j.ydbio.2015.10.034
0012-1606/

primordium is composed of < 100 cells of two primary types; b) once patterned, DA-tube cells do not divide, die, or recruit new cells during DA-tube elongation; and c) DA-tubes are branchless and do not elaborate beyond bending and flattening the lumen into a shape resembling a hockey stick. Second, the product of this process, the DA itself, reveals the shape of the terminal DA-tube

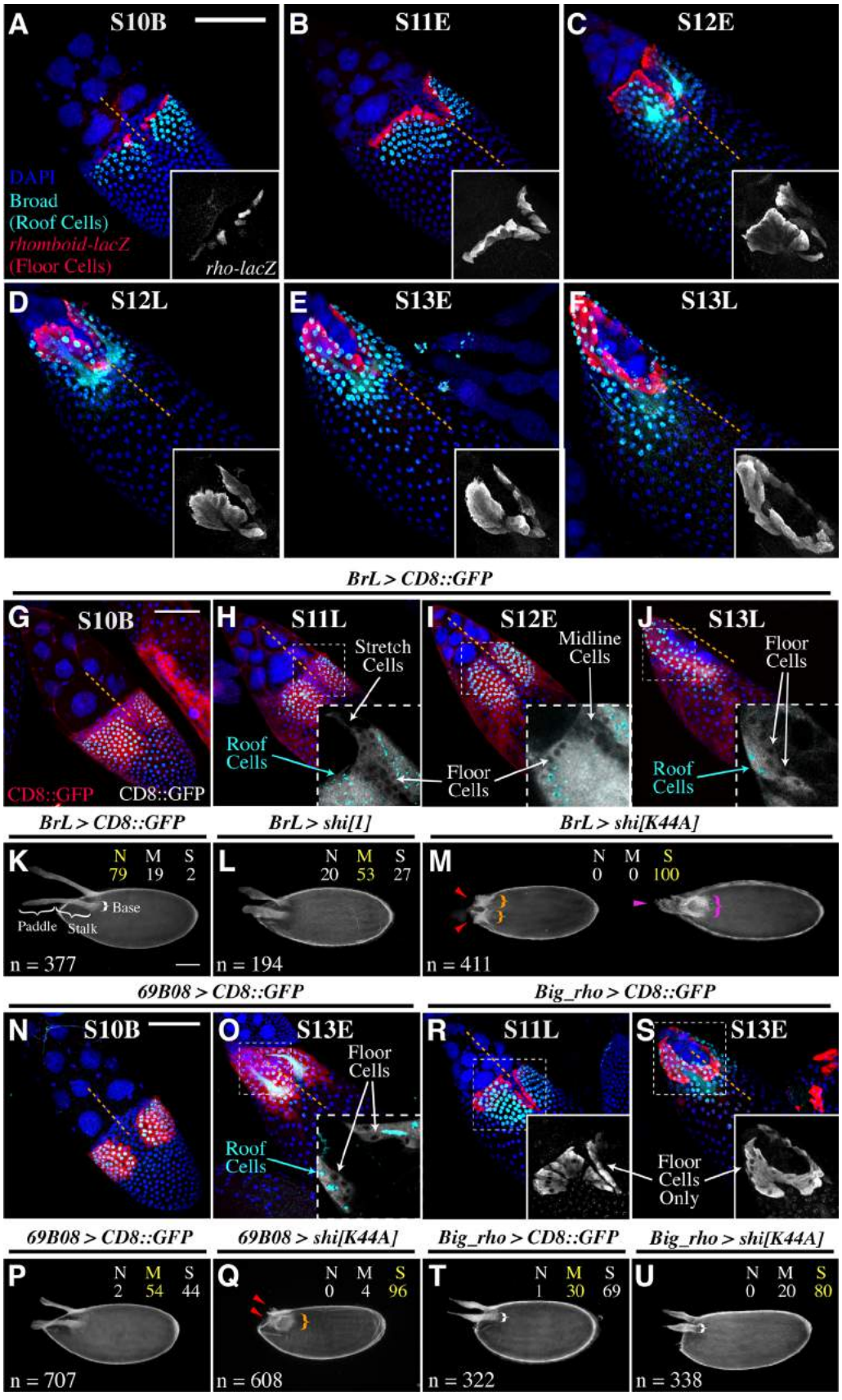

lumen and reflects any defects that may have occurred during DA tubulogenesis. Finally, the site of DA tubulogenesis, the fly ovary, is genetically tractable, easily accessible via dissection, and readily amenable to microscopy; furthermore, each ovary contains a distribution of all egg-chamber stages, providing a wealth of tubulogenic material for analysis of fixed or living tissue. These features have facilitated the study of DA-tube-cell patterning (e.g., Tzolovsky et al., 1999; Ward and Berg, 2005; Yakoby et al., 2008; Bosclair Lachance et al., 2009; Boyle and Berg, 2009; Andreu et al., 2012; Fuchs et al., 2012), DA-tube formation (Dorman et al., 2004; Osterfield et al., 2013), and DA-tube elongation (Dorman et al., 2004; Boyle et al., 2010; Peters et al., 2013). Thus, the *Drosophila* ovary provides an ideal system for understanding how the regulation of cell shape, rearrangement, adhesion, and migration contribute to epithelial tube formation and elongation.

DA tubulogenesis occurs during the late stages of oogenesis (S10—S14), shortly after the follicle cell (FC) epithelium that encases each cluster of germ cells receives signals that specify two dorsal primordia of DA-forming cells (S10B; Fig. 1A). This patterning relies on the intersection of epidermal growth factor receptor (EGFR) and bone morphogenetic protein (BMP) pathways within the FC epithelium of each egg chamber, providing a combinatorial framework for establishing precise spatial and temporal gene-expression patterns (summarized in Yakoby et al., 2008). By S10B, each DA primordium contains two major cell types: *broad*-expressing "roof" cells that form the outward-facing roof and sides of the DA tube, and *rhomboid*-expressing "floor" cells that seal off the floor of the DA tube (Fig. 1A; Dorman et al., 2004; Ward and Berg, 2005). As egg chambers transition from S10B to S11, roof cells initiate apical constriction from the anterior to posterior, and the floor cells, which form a single, hinge-shaped row anterior and dorsal to the roof cells, begin to buckle (Fig. 1B). As S11 transitions to S12, roof FC apices constrict down to their smallest size while the floor cells dive underneath the roof cells, flipping their apical–basal orientation, and zipper together to seal the DA-tube (Fig. 1C; Dorman et al., 2004; Osterfield et al., 2013). This wrapping process, which resembles primary vertebrate neurulation, forms each of the rudimentary DA tubes (first visible in Fig. 1C). Once each DA tube forms, the DA-tube cells rearrange, expand their apices, and migrate over the adjacent, squamous, stretch cells towards the anterior end of the egg chamber, elongating the tube (S12—13; Fig. 1D–F; Tran and Berg, 2003; Dorman et al., 2004). Throughout DA tubulogenesis, the DA-tube cells, which are oriented with their basal faces out and apical faces in, secrete eggshell protein into the DA-tube lumens to form the DAs of the eggshell (Fig. 1C–F).

While characterizing the transcriptional regulation of DA-tube elongation, we discovered that Tramtrack69 regulates the expression of *shibire* (*shi*) in FCs at the transition from tube formation to tube expansion (Peters et al., 2013); *shi* encodes *Drosophila* Dynamin (van der Bliek and Meyerowitz, 1991). Since Dynamin has known roles in other morphogenetic contexts (e.g., Pirraglia et al., 2006; Pirraglia et al., 2010; Fabrowski et al., 2013; Gomez et al., 2012; Lepage and Bruce, 2014; Lee and Harland, 2010; Ogata et al., 2007; Bogdanovic et al., 2012; Lee et al., 2014; Gray et al., 2005), and functional RNAi studies indicate that Dynamin promotes DA elongation (Peters et al., 2013), we decided to delve deeper into Dynamin's role in DA tubulogenesis.

Dynamin is a large GTPase that is best known for its ability to self-assemble into multimeric rings around the necks of clathrin-coated membrane pits and, through enhanced GTP hydrolysis provided by this conformation, to exert the mechanical force necessary for vesicle scission during endocytosis (Chappie et al., 2011; Chappie and Dyda 2013). Dynamin's role is not limited to clathrin-mediated endocytosis, however, but extends to a wide variety of cellular processes including alternative endocytic pathways and intracellular budding (Furgeson and De Camilli, 2012), regulation of actin and microtubule dynamics (Sever et al., 2013), centrosome cohesion (Thompson et al., 2004), and apoptosis (Soulet et al., 2006).

Here, we explore the role of Dynamin in DA tubulogenesis, and we demonstrate that disruption of Dynamin function in DA-tube cells leads to defects in DA-tube closure, DA-tube-cell rearrangement, and planar-polarized apical membrane expansion during DA-tube elongation. Furthermore, we provide evidence that Dynamin promotes these movements by regulating endocytosis. Consistent with this claim, we observe mis-localized E-cadherin and Integrin following Dynamin disruption, and we present functional data consistent with a model in which Dynamin promotes DA-tube elongation through endocytic remodeling of cellular adhesions.

2. Materials and methods

2.1. Drosophila strains

We used the following strains, which are available from the Bloomington Stock Center (BL) or the Vienna Drosophila Resource Center, VDRC (V) and are described in FlyBase (http://flybase.bio.indiana.edu/): *UAS-shi[K44A]* (dominant-negative Dynamin; BL5811), *UAS-mCD8::GFP* (negative control; BL5137), *UAS-Rab5 [S43N]* (dominant-negative Rab5; BL42703), *UAS-mCherry* RNAi (RNAi negative control; BL35785), *UAS-Rab5* RNAi (BL34832), *UAS-AP50* RNAi (BL28040), *UAS-shotgun* RNAi (E-Cadherin RNAi; V27082), *UAS-myospheroid* RNAi (βPS-Integrin RNAi; V29619), *br [69B08]-GAL4* (Jenett *et al.*, 2012, BL39481). The following strains were gifts: *w*; brL-GAL4; tub-gal80[ts]/TM3* (S. Shvartsman), *w*;; 20XUAS-TTS-shi[1]* (temperature-sensitive Dynamin; Pfeiffer et al., 2012, via A. Sustar), *y* w**; *shg::GFP* (endogenous E-Cadherin::GFP; Huang et al., 2009, via M. Osterfield), *y* w**; *UASP-shi::YFP* (Dynamin::YFP; Fabrowski et al., 2013, via S. De Renzis), *w*;; UAS-shg::GFP* (E-Cadherin::GFP; Oda and Tsukita 1999, via S. Hou), *w*;; UAS-βPS-Integrin(mys), UAS-PS1-Integrin(mew)* and *w*;; UAS-βPS-Integrin(mys),* and *UAS-PS2-Integrin(if)* (Beumer et al., 1999; Beumer et al., 2002, via K. Broadie). *Vm26Aa-GAL4* is described in Peters et al., 2013. *Big_rho-GAL4* includes regulatory DNA from the *rhomboid* promoter that drives floor-cell-specific GAL4 expression from S11—S14 (contact C. Berg for more details). To visualize floor cells, we used *y* w *; P{w+mC=rho(ve)-lacZ.0.7}* (*rhomboid-lacZ* reporter; Ip et al., 1992).

Fig. 1. Expression of dominant-negative Dynamin in DA-tube cells disrupts DA tubulogenesis. (A–F) Staged *rhomboid-lacZ* egg chambers, stained for Broad protein (roof cell nuclei – cyan), ß-Galactosidase (floor cells – red; white in insets), and DNA (DAPI – blue), illustrate the cooperative movements of roof and floor cells during DA tubulogenesis (S10B—S13L). Images are oriented with the anterior facing upper left. Dotted orange lines indicate dorsal midlines. (G–J) Control *brL > CD8::GFP* egg chambers raised at 30 °C, stained for Broad protein (cyan), CD8::GFP (red; white in insets), and DNA (blue), illustrate the spatial extent of GAL4 expression at this temperature. Insets highlight CD8::GFP expression in Broad-positive roof cells and adjacent, Broad-negative floor cells, midline cells, stretch cells, etc. (K–M) Laid eggs from control *brL > CD8::GFP* (K), *brL > shi [1ts]* (L), or *brL > shi[K44A]* (M) females, raised at 30 °C. In K, the parts of a wild-type DA are labeled (paddle, stalk, base). Numbers indicate percentages of normal or mildly defective (N), moderately defective (M), and severely defective (S) DAs; yellow numbers indicate the category of egg being shown. The number of eggs scored for each condition is shown in the lower left of each panel. Red arrowheads indicate abnormally wide DAs, orange brackets indicate abnormally wide DA bases, purple arrowheads indicate DA fusions, and purple brackets indicate fused DA bases. (N, O) Control *br[69B08] > CD8::GFP* egg chambers raised at 30 °C, stained for Broad protein (cyan), CD8::GFP (red; white in insets), and DNA (blue), illustrate the spatial extent of GAL4 expression. Inset in O shows CD8::GFP expression in roof cells and adjacent floor cells only. (P, Q) Laid eggs from control *br[69B08] > CD8::GFP* (P) or *br[69B08] > shi[K44A]* (Q) females raised at 30 °C. (R, S) Control *Big_rho > CD8::GFP* egg chambers raised at 30 °C, stained for Broad protein (cyan), CD8::GFP (red; white in insets), and DNA (blue), illustrate the spatial extent of GAL4 expression. Insets demonstrate that CD8::GFP expression is restricted to floor cells only. (T, U) Laid eggs from control *Big_rho > CD8::GFP* (T) or *Big_rho > shi[K44A]* (U) females raised at 30 °C. Scale bars = 100 μm. E = early, L = late.

2.2. Tissue-specific expression: GAL4-UAS

To obtain ovaries and eggs, we crossed *GAL4*-bearing virgin females to *UAS*-bearing males at 25 °C, or at 18 °C if the *GAL4-UAS* combination resulted in lethality at 25 °C. In this study, except for the 25 °C and 28 °C experiments represented in Fig S1 and Fig. 4, respectively, we mated the F1 females to w^{1118} males at 30 °C to produce the strongest GAL4 expression and most consistent phenotypes, and we included wet yeast to maximize egg and egg chamber production. After >24 h at 30 °C, we collected eggs over successive 8-12-hr periods on apple juice/agar plates, then rinsed, pooled, and mounted the eggs in Hoyer's medium (van der Meer, 1977). If a *GAL4-UAS* combination perturbed egg-laying, we dissected ovaries, fixed in 4% para-formaldehyde for 20 min, dissociated ovaries, and proceeded either with immunostaining or with eggshell preparation in Hoyer's medium. In some assays (Figs S1 and 4), to produce more moderate defects or to determine which DA features were most sensitive to perturbation, we collected eggs from flies kept at 25 °C or 28 °C. In addition to qualitative descriptions, we evaluated DA defects using a three-tiered scoring system (N=normal DAs or DAs with mild defects, M=moderate DA defects, S=severe DA defects), counting a minimum of 100 eggs (mean=312 eggs). Moderate defects included rough/feathered DA shape, a difference in DA length within the DA pair, wide DA paddles, shafts, or bases, and short DAs that extended past the micropyle. Severe DA defects included short and/or wide DAs that did not extend past the micropyle, fused DAs, or a combination of moderate defects.

To assess the tissue-specificity of our DA-tube GAL4 drivers (*brL-GAL4; tub-gal80[ts]*, *br[69B08]-GAL4,* and *Big_rho-GAL4*), we compared localization of GAL4-driven CD8::GFP and Broad protein (roof cells) for these lines (Fig. 1G–J, N, O, R, S; Fig S1A–D). For *brL-GAL4; tub-gal80[ts]* at 25 °C, we detected CD8::GFP in Broad-positive roof cells, as expected, but also in the adjacent, Broad-negative floor cells (Fig S1A–D); at 30 °C, we detected high CD8::GFP in both Broad-positive roof cells and Broad-negative floor cells, but we also found CD8::GFP in other anterior, Broad-negative FC types (e.g., midline cells and stretch cells) and main-body FCs posterior and ventral to the DA primordia (Fig. 1G–J). For *br[69B08]-GAL4* at 30 °C, we detected CD8::GFP only in Broad-positive roof cells and adjacent, Broad-negative floor cells (Fig. 1N, O). For *Big_rho-GAL4* at 30 °C, we detected CD8::GFP only in Broad-negative floor cells (Fig. 1R, S).

Background defects associated with GAL4-driven CD8::GFP expression were lowest for *brL-GAL4; tub-gal80[ts]* (9% moderate at 25 °C; Fig. S1E; 19% moderate and 2% severe at 30 °C; Fig. 1K), relative to *br[69B08]-GAL4* (54% moderate and 44% severe at 30 °C; Fig. 1P) and *Big_rho-GAL4* (30% moderate and 69% severe at 30 °C).

2.3. Immunostaining

Ovary immunostaining was as described (Ward and Berg, 2005; Zimmerman et al., 2013), except that permeabilizations were performed with 2% Triton in PBT (PBS+0.1% Tween). Antibodies used were rabbit anti-β-galactosidase (pre-adsorbed 1:500, 1:10,000 final dilution; Cappel), rabbit anti-GFP (1:200, Molecular Probes), mouse anti-BR-core (1:250, 25E9.D7-concentrate, Developmental Studies Hybridoma Bank, DSHB; Emery et al., 1994), rat anti-α-E-cadherin (1:50, DCAD2-concentrate, DSHB; Oda et al., 1994), mouse anti-α-Spectrin (1:50, 3A9-concentrate, DSHB; Dubreuil et al., 1987), mouse anti-β-PS-Integrin (1:50, CF.6G11-concentrate, DSHB; Brower et al., 1984), rabbit anti-Dynamin (1:100, Ab 2074, via M. Ramaswami; Estes et al., 1996) and goat anti-mouse Alexa Fluor 488-, 555-, and 647-conjugated antibodies (1:500, Molecular Probes). Imaging was performed on either a Zeiss 510 or Leica SP8X scanning confocal microscope (immunostaining, live imaging), or a Nikon Microphot FXA (eggshells). Images were processed using Helicon Focus (Helicon Soft Ltd.) and FIJI (ImageJ-based, NIH; Schneider et al., 2012).

2.4. Quantitative cytology

To quantify the dimensions of Broad-expressing roof FC primordia (Fig. 3A–K), we made the following measurements using FIJI (ImageJ). For anterior–posterior (AP) length, we made a maximum-intensity *XY* projection of each egg chamber and measured the length from the most anterior to the most posterior roof FC nucleus. For dorsoventral (DV) width, which occurs along a curved surface, we made a 3D projection of each egg chamber around the *Y* axis, rotated the projection to view the egg chamber head on, and measured the circumferential distance from the most dorsal to the most ventral roof FC nucleus in each primordium (inset in Fig. 3K). For each condition at each stage, we measured a minimum of 10 primordia (mean=12 primordia), and for AP:DV ratios we only used primordia for which we could obtain both AP and DV measurements.

To quantify the apical dimensions and surface area of anterior and posterior roof FC apices (Fig. 3L–W), we made the following measurements using FIJI (ImageJ). For anterior and posterior roof FC apices, we chose ~3 non-adjacent cells in the front 1/3 or rear 1/3 of each roof FC primordium, respectively (Fig. 3 L–U), and we only measured apices for which we could achieve a view perpendicular to the apical plane. For each apical surface, we measured AP and DV lines that intersected at their midpoints and at the center of the apical surface (inset in Fig. 3V), and we traced the outline of the apical surface and measured the area (inset in Fig. 3W). For each condition at each stage, we measured a minimum of 20 apices (mean=47 apices).

For statistical analyses, we compared means using ANOVA and Tukey's posthoc tests.

2.5. Live imaging

We dissected ovaries from flies raised at 30 °C in Schneider's medium (S2 cell culture medium; Sigma) that was equilibrated to 30 °C, and we then combed the ovarioles apart. We carefully squeezed individual S10B egg chambers out of the ovariole muscle sheath to avoid complications from muscle contractions during live imaging. Once liberated, we transferred these S10B egg chambers to fresh 30 °C S2 medium in a coverslip-bottomed 35 mm culture dish (MatTek Corp.) that had already been positioned on an inverted-objective, scanning confocal microscope. During subsequent steps, the temperature of the medium was allowed to fall to room temperature, ~22 °C. We brushed the egg chambers into the center of the coverslip, soaked and sank a small (~1 cm × 1 cm) piece of KimWipe (Kimtech) into the S2 medium and positioned it over the egg chambers like a blanket. We placed a small (>1 cm diameter) brass washer over the KimWipe such that it surrounded, but did not lie on top of, the egg chambers. This weight provided just enough downward force on the egg chambers to keep them in place without crushing them, a precaution that was particularly necessary because DA-tube elongation is a forceful process, and DA-tube cells will easily push an unanchored egg chamber away from the coverslip. Once anchored, we selected the best S10B or S11 dorsal- or dorsolateral-oriented egg chamber and collected Z-stacks for 10 h at 8-min or 15-min time intervals. We subsequently processed the movies in Imaris (Bitplane, Oxford Instruments).

3. Results

3.1. Dynamin's GTPase activity is required in DA-tube roof cells for DA tubulogenesis

To characterize Dynamin's role in DA tubulogenesis, we disrupted its function by expressing dominant-negative (DN), GTP-hydrolysis-defective forms of Dynamin in DA-tube cells via the

GAL4-UAS system (Brand and Perrimon, 1993; see methods). We expressed either *shibire[1ts]*, which encodes a protein that is functional at 25 °C and dominant negative at 30 °C (van der Bliek and Meyerowitz, 1991) or, in most cases, *shibire[K44A]*, which encodes a protein that is constitutively dominant negative (van der Bliek et al., 1993). For GAL4 driver lines, we used either *brL-GAL4; tub-gal80[ts]* (roof, floor, and adjacent FCs), *br[69B08]-GAL4* (roof and floor cells only), or *Big_rho-GAL4* (floor cells only) (Fig. 1, S1; see methods for details on GAL4-driver tissue specificity). To assess DA defects, we scored eggshell DAs as either normal (N), moderately defective (M) or severely defective (S), and presented the proportions of each category with representative eggshell images (see methods).

DAs of *brL > CD8::GFP* control eggs exhibited wild-type DA morphology (i.e., a narrow stalk connected to a widened, anterior paddle; Fig. 1K, S1E) with only a slight reduction in DA length relative to wild type. DAs of *brL > shi[1ts]* eggs were indistinguishable from controls at the permissive temperature of 25 °C (compare Fig. S1 E–F), and were notably shorter and wider than controls at the restrictive temperature of 30 °C (compare Fig. 1K to L), demonstrating that *functional* Dynamin plays a role in DA tubulogenesis. DA defects of *brL > shi[K44A]* eggs produced at 25 °C, when *brL-GAL4* expresses in only roof and floor cells (Fig. S1A–D), were similar in frequency and severity to those of *brL > shi[1ts]* eggs at 30 °C (compare Figs. S1G to 1 L), indicating a tube cell-specific role for Dynamin in DA tubulogenesis; at 30 °C, DA defects of *brL > shi[K44A]* eggs were more dramatic and fully penetrant (Fig. 1M), consistent with previous observations that the degree of *shi[K44A]*'s disruptive effect depends on expression level (Moline et al., 1999). These DAs were short, wide, and flat, had rough, irregular edges, wide bases, and were often fused (Fig. 1M,); short, wide DAs suggest a defect in DA-tube elongation, while the wide DA bases and DA fusions suggest a defect in DA-tube formation. These results indicate that DA-tube cells require functional Dynamin for DA tubulogenesis and suggest that Dynamin functions in both DA-tube formation and elongation.

Since *brL-GAL4* at 30 °C drives expression in both DA-tube cells and adjacent FC types (Fig. 1G–J), we tested other *br-GAL4* drivers and found that *br[69B08]-GAL4* drives expression only in roof and floor cells at 30 °C; Fig. 1N, O. Control *br[69B08] > CD8::GFP* eggs had a higher proportion of background DA defects than control *brL > CD8::GFP* eggs, but these defects were primarily associated with DA length, not width or shape (compare Fig. 1K–P). In contrast, the DAs of *br[69B08] > shi[K44A]* eggs, just as those of *brL > shi[K44A]* eggs, were severely stunted, flat, wide, and irregular in shape (compare Fig. 1M–Q). We did observe fewer DA fusions on *br[69B08] > shi[K44A]* eggs than *brL > shi[K44A]* eggs, potentially due to differences in midline-cell GAL4 expression (compare Fig. 1G–N). Taken together, these results demonstrate that the DA-tube cells themselves (i.e., roof and floor cells) require functional Dynamin for DA tubulogenesis.

To distinguish between tubulogenic requirements for Dynamin within subsets of the DA-tube cells (i.e., roof cells vs. floor cells), we compared the effects of *br[69B08] > shi[K44A]* expression (roof and floor cells; Fig. 1N, O) to *Big_rho > shi[K44A]* expression (floor cells only; Fig. 1R, S). We are unaware of a GAL4 driver that is entirely specific to roof cells; because *Big_rho-GAL4* expression is floor-cell specific, however, and since *Big_rho-GAL4* can serve as a tool to perturb DA tubulogenesis (Altaras et al., in preparation), we reasoned that a comparison between *br[69B08] > shi[K44A]* and *Big_rho > shi[K44A]* eggs should allow us to assess the relative contribution of roof cell-Dynamin to DA tubulogenesis. Control *Big_rho > CD8::GFP* eggs exhibited background defects in DA length and shape: DAs were short, thin, and pointed (Fig. 1T), corresponding to subtle but consistent differences in floor cell morphology (compare Fig. 1E–S). DAs of *Big_rho > shi[K44A]* eggs closely resembled those of controls (Fig. 1U), with only a small increase in penetrance of DA defects. Notably, we did not observe the flat, wide-based DAs that we observed on *brL > shi[K44A]* and *br[69B08] > shi[K44A]* eggs that were indicative of DA-tube formation defects.

Altogether, these GAL4 experiments support a role for Dynamin in DA-tube cells in promoting both DA-tube formation and elongation, and suggest that Dynamin's activity is most critical in the roof cells. Dynamin activity in floor cells is either not required for DA-tube formation or is more recalcitrant to our perturbation methods. Of these GAL4 conditions, we selected *brL > shi[K44A]* for all further characterizations of underlying cellular and molecular defects, because the background defects of *brL-GAL4* were the least severe of all GAL4 lines tested, and because our data demonstrate that *brL > shi[K44A]* at 30 °C is an effective and penetrant method for disrupting Dynamin function and DA tubulogenesis.

3.2. Dynamin is required for DA-tube closure

The formation of the DA tube requires the cooperative actions of two distinct, juxtaposed cell types: roof FCs and floor FCs (Fig. 1A–F; Dorman et al., 2004, Ward and Berg, 2005, Osterfield et al., 2013). To evaluate the tissue and cellular impacts of disrupting Dynamin function, we compared floor FC morphology (*rhomboid-lacZ* marker – *rho-lacZ*) throughout DA tubulogenesis (S11—S14) in *brL-GAL4 > CD8::GFP* and *brL > shi[K44A]* egg chambers (Fig. 2). We observed no obvious differences between control *brL > CD8::GFP* and *brL > shi[K44A]* egg chambers during S10B, indicating that *brL > shi[K44A]* expression did not affect floor-cell patterning (data not shown), or early in S11, when DA tubulogenesis begins (compare Fig. 2A to F). By early S12, however, the first differences between *brL > CD8::GFP* and *brL > shi[K44A]* egg chambers were apparent: whereas control floor FCs had sealed together to complete tube formation (Fig. 2B), the floor FC hinge in Dynamin[DN] egg chambers remained open (Fig. 2G). By late S12, control floor FCs had shortened along their apical–basal axes and were migrating anteriorly over the dying nurse cells (Fig. 2C). As a result, the distance between the two primordia increased along the dorsal midline, especially near the DA bases. These movements proceeded through S13 (Fig. 2D) and S14 (Fig. 2E), with the DA tube remaining sealed throughout this time (orange arrows), until the floor FCs were arranged in two rows along the AP axis and had adopted the shape of the finished DA tube (Fig. 2E). In contrast, floor FCs in *brL > shi[K44A]* egg chambers did not change shape or move anteriorly over the nurse cells, although they still attempted to migrate in an anterior direction (inset in Fig. 2J). Furthermore, the two primordia stayed in contact along the dorsal midline (Fig. 2I), and the DA tubes remained unsealed (Fig. 2G–J, orange dotted lines). Indeed, we never observed an instance of DA-tube closure in *brL > shi[K44A]* egg chambers from S12—S14 ($n=95$). These data demonstrate that Dynamin plays an essential role in DA-tube closure.

3.3. Dynamin is required for roof-FC intercalation during DA-tube elongation

To reveal dynamic cellular behaviors that could explain the DA defects we observed on *brL > shi[K44A]* eggs, and to determine whether *brL > shi[K44A]* expression affected the viability of DA-tube cells, we examined DA tubulogenesis live using an E-Cadherin::GFP knock-in strain (Huang et al., 2009). We compared control egg chambers that also expressed *brL-GAL4* (Movies S1 and S2) to Dynamin[DN] egg chambers expressing both endogenous E-Cadherin::GFP and *brL > shi[K44A]* (Movies S3 and S4). In control egg chambers, roof-cell apical constriction and DA-tube formation were quickly followed by intercalation and dramatic,

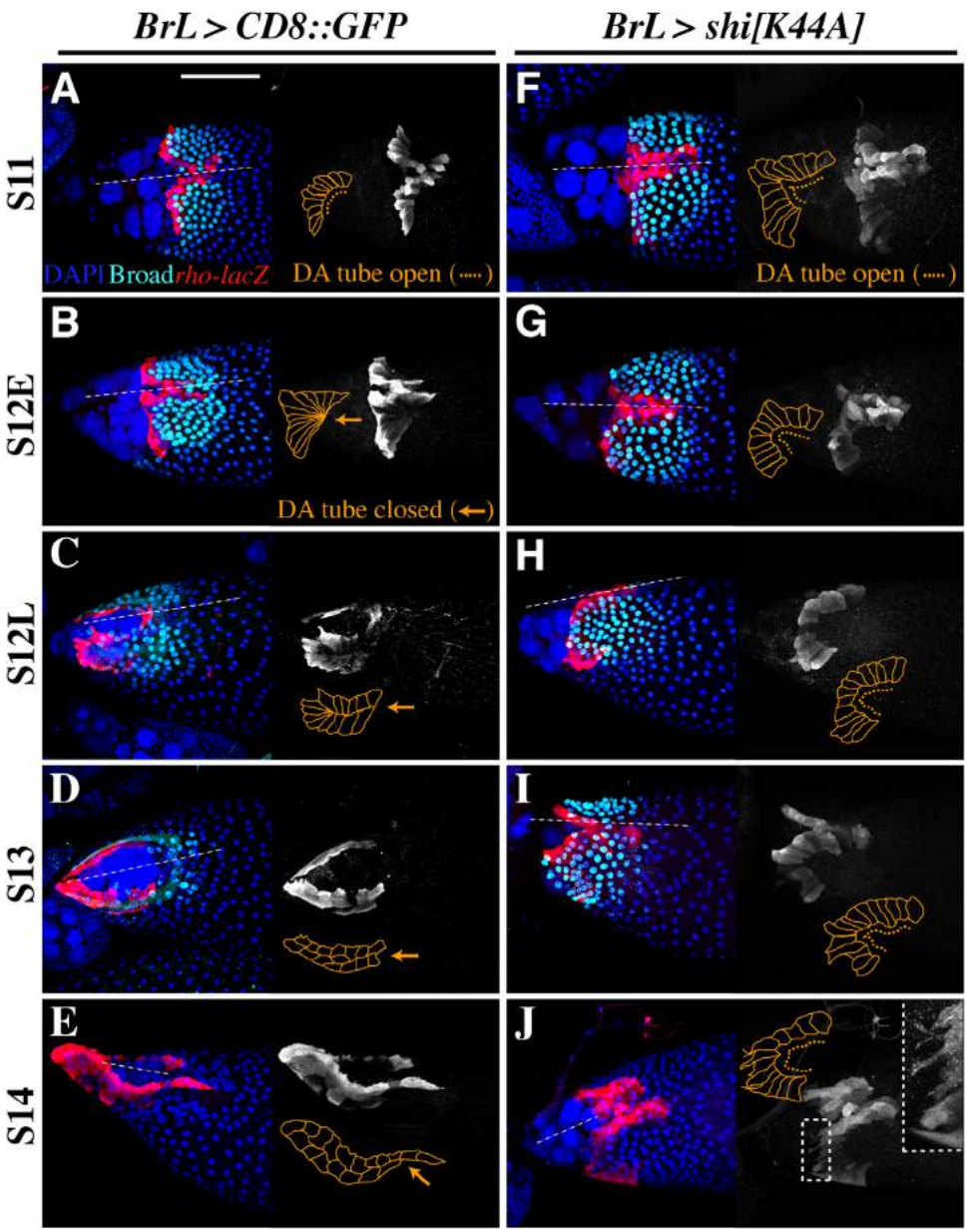

Fig. 2. Expression of dominant-negative Dynamin in DA-tube cells disrupts DA-tube closure. (A–J) Anterior views of S11—S14 control *brL > CD8::GFP* (A–E) vs. *brL > shi[K44A]* (F–J) egg chambers, stained for DNA (DAPI – blue), Broad protein (roof-FC nuclei – cyan), and β-galactosidase produced by *rhomboid-lacZ* (floor cells – red or white). Each panel also includes an orange tracing of floor cell outlines for a single DA tube, with orange dotted lines indicating an open DA tube and orange arrows indicating a sealed DA tube. Note that while control DA tubes have closed by S12E (B) and remain closed (C–E), dominant-negative-Dynamin-expressing DA tubes fail to close (F–J), although floor cell leading edges still attempt anterior migration (inset in J). Scale bar = 50 μm.

anterior DA-tube elongation (Movies S1 and S2). Between 7–9 hours after DA-tube formation, we observed significant eggshell secretion, indicating that our culturing conditions were not affecting egg chamber viability (Movie S2). In E-Cadherin::GFP *brL > shi[K44A]* egg chambers, apical constriction occurred normally as in controls, but in contrast to controls, the DA tubes did not narrow and elongate along the DV axis; each patch remained wide and appeared disorganized, reflecting the DA-tube-formation defects we observed in fixed tissue (Fig. 2; Movies S3 and S4). Roof-cell apical expansion occurred at the expected time, but DA-tube-cell apices did not properly intercalate, and DA-tube elongation was severely impaired and disordered (Movies S3 and S4). In some cases, we observed fusion of DA-tube material (Movie S4), consistent with DA fusions we observed on laid eggs (Fig. 1M). Importantly, eggshell secretion occurred at a time comparable to controls (compare Movie S2 to S3 or S4). Interestingly, we also noted altered behavior of E-Cadherin in *brL > shi[K44A]* egg chambers; E-cadherin accumulated in apical "blobs", which appeared prior to and during eggshell secretion (Movies S3 and S4). These live-imaging data demonstrated that *brL > shi[K44A]* expression did not affect FC viability or eggshell secretion but did affect E-Cadherin behavior; these data also suggested that defects in DA-tube-cell intercalation might underlie the observed DA-tube elongation defects.

Supplementary material related to this article can be found online at http://dx.doi.org/10.1016/j.ydbio.2015.10.034

Prior to DA tubulogenesis, each roof FC primordium is wider along the DV axis than it is along the AP axis; during DA-tube elongation, the primordia shrink in width and extend in length as the roof FCs intercalate (Dorman et al., 2004; Ward and Berg, 2005). To ascertain the underlying mechanisms that contribute to Dynamin[DN]-associated tube-elongation defects, we

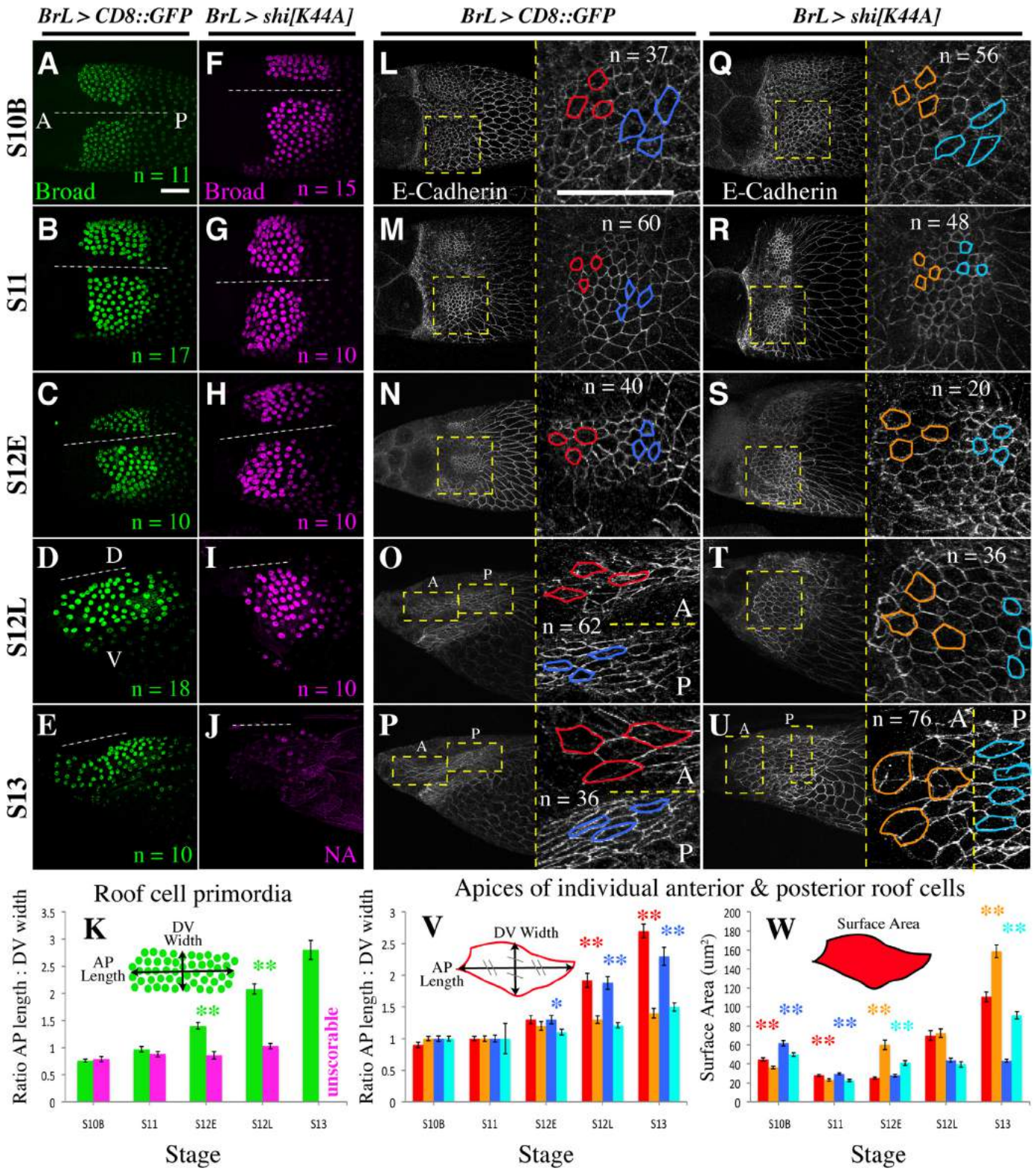

Fig. 3. Expression of dominant-negative Dynamin in DA-tube cells disrupts roof FC intercalation and anterior-biased apical expansion. (A–J, L–U) Anterior views of S10B–S13 control *brL > CD8::GFP* (A–E, L–P) vs. *brL > shi[K44A]* (F–J, Q–U) egg chambers, stained for Broad protein (roof-FC nuclei – green A–E, magenta F–J), and E-Cadherin (FC apices – L–U white). Broad and E-Cadherin stains were administered on the same egg chamber (e.g., A and L, F and Q). The number of egg chambers scored for each condition is shown in the lower right of panels A–J. (L–U) Full-sized images (left) are accompanied by enlarged insets of roof-FC apices (right), and labeled A (anterior) or P (posterior) if the enlargement is split. In enlarged panels, representative examples of anterior (red or orange) or posterior (blue or cyan) apices are outlined, and the total number of apices compared for each condition is indicated. (K, V) Mean AP length: DV width ratios, ± standard error, for roof-FC primordia (K) or roof-FC apices (V) as a function of stage (S10B—S13). (W) Mean surface area, ± standard error, for roof-FC apices as a function of stage (S10B—S13). Insets in K, V, and W indicate how AP length, DV width, or apical surface area were measured (see also methods); asterisks indicate statistical differences (*$=p<0.05$, **$=p<0.001$, and asterisk color indicates which value was greater (green vs. magenta, red vs. orange, blue vs. cyan)). Colors are consistent between images (A–J, L–U) and charts (K, V, W). Scale bars=50 μm.

tested whether *brL > shi[K44A]* expression affected roof FC patterning or intercalation (Broad protein stains; Fig. 3A–K).

We first asked whether disrupting Dynamin function had any effect on roof-FC patterning. We compared the number of BR-positive nuclei in *brL > CD8::GFP* control and *brL > shi*[K44A] egg chambers between S10B—S12 (once patterned, the number of BR nuclei remain constant; Ward and Berg, 2005). We found no significant difference ($p > 0.1$) between the number of BR-positive nuclei in *brL > CD8::GFP* control egg chambers (67 nuclei per primordium, $n = 49$) and *brL > shi[K44A]* egg chambers (65 nuclei per primordium, $n = 35$), indicating that *brL > shi[K44A]* does not affect roof FC patterning as revealed by BR protein expression.

To compare the dimensions of the roof-FC primordia, we measured the ratio of AP length to DV width in control and *brL > shi[K44A]* roof-FC primordia from S10B—S13 (see methods and schematic in Fig. 3K). As expected, we observed that roof FCs in S10B control *brL > CD8::GFP* egg chambers were positioned on either side of the dorsal midline and that the DV width was greater than the AP length (AP:DV ratio = 0.8, Fig. 3A, first green bar in K). By S11, the AP:DV ratio was 1; by the end of S12, it had increased to 2.1; and by the end of S13, roof FC primordia were 2.8 times longer than they were wide, indicating substantial roof-FC reorganization during DA-tube expansion (Fig. 3B–E, green bars in K). In *brL > shi[K44A]* egg chambers, the roof-FC primordia at S10B resembled controls, with similar position and AP:DV character (AP:DV ratio = 0.8, Fig. 3F, first magenta bar in K), but during S11—S14, the roof-FC nuclei remained relatively static and did not reorganize along the AP axis (Fig. 3G–J, magenta bars in K, green asterisks indicate $p < 0.001$). We could not measure roof-FC primordia dimensions in S13 and older *brL > shi[K44A]* egg chambers because the BR signal was too weak and variable (Fig. 3J and K). This apparent early loss of Broad protein in S13 *brL > shi[K44A]* egg chambers could suggest that Dynamin helps maintain Broad nuclear localization. Alternatively, these egg chambers were actually older, but neither nurse-cell death nor DA-tube elongation had proceeded normally. Together, these observations suggest that in addition to floor FCs requiring Dynamin function during DA-tube formation, roof FCs require Dynamin function to intercalate during DA-tube elongation.

3.4. DA-tube elongation involves AP-biased apical expansion, which requires functional Dynamin

Concomitant with roof-FC intercalation and DA-tube elongation, the apical surfaces of DA-tube cells expand, increasing the volume of the tube and elongating the tubes toward the anterior of the egg chamber (Dorman et al., 2004; Boyle et al., 2010). To compare the apical membrane morphology and behavior of roof FCs in control and *brL > shi[K44A]* egg chambers, we measured the ratio of apical AP length to apical DV width, as well as apical surface area, for individual roof FCs from S10B—S13. We compared 3 non-adjacent apices in the anterior (Fig. 3, red vs. orange) and 3 non-adjacent apices in the posterior (Fig. 3, blue vs. cyan) of each roof-FC primordium (see methods, enlargements in Fig. 3L–U, charts in V and W). This detailed quantification of roof-FC apical behavior during DA tubulogenesis revealed a striking planar-polarized elongation of roof cells during tube expansion.

In *brL > CD8::GFP* control egg chambers at S10B, at the first initiation of roof-FC apical constriction, anterior apices (45 μm^2) began to constrict slightly before posterior apices (62 μm^2), and both anterior apices (0.9) and posterior apices (1.0) maintained a nearly equivalent AP:DV ratio (Fig. 3L, V, W; see also Dorman et al., 2004). In S11, constricted anterior (28 μm^2) and posterior (30 μm^2) apices were almost identical in area (Fig. 3M and W), and the cells maintained an equivalent AP:DV ratio of 1.0 (Fig. 3M and V). By early S12, as overlying roof FC nuclei began to rearrange and extend along the AP axis (Fig. 3C), anterior (25 μm^2) and posterior (28 μm^2) apices remained tightly constricted, but their shapes began to change from hexagonal to rhomboidal, resulting in an increase in AP:DV ratio (both = 1.3, Fig3 N, V, W). By late S12, anterior apices had substantially expanded (70 μm^2) while posterior apices (44 μm^2) had expanded to a lesser degree (Fig. 3O and W), though again, cell shapes exhibited an equivalent AP:DV ratio of 1.9. These results suggest that both anterior and posterior cells within the primordium expand in an AP-biased direction (Fig. 3O, V). By S13, the behavior of anterior apices had diverged from that of posterior apices. Anterior apices, which form the DA paddle, had expanded dramatically (111 μm^2), almost 3 times that of posterior apices (40 μm^2), which make the stalk, and the AP:DV ratio of anterior vs. posterior apices was 2.7 vs. 2.3, respectively (Fig. 3P, V, W).

In *brL > shi[K44A]* egg chambers at S10B, as in controls, anterior apices (36 μm^2) began to constrict slightly before posterior apices (50 μm^2), and both anterior apices (1.0) and posterior apices (1.0) maintained equivalent AP:DV ratios (Fig. 3Q, V, W). Interestingly, both anterior and posterior apical areas were significantly smaller than these areas in controls ($p < 0.001$). In S11, constricted anterior (23 μm^2) and posterior (23 μm^2) apices maintained an equivalent AP:DV ratio of 1.0 (Fig. 3R, V, and W) and were again significantly smaller than controls ($p < 0.001$). This smaller apical surface area could be due to *shi[K44A]* over-stimulating the apical constriction machinery, as shown in vertebrate cell culture (Chua et al., 2009), or it could be due to smaller overall egg chamber size. Consistent with the latter possibility, we found that S11 *brL > shi[K44A]* egg chambers were ~5% shorter than controls (482 μm vs. 506 μm, $n = 12$, $p < 0.05$). By early S12, however, Dynamin[DN] egg chambers had reversed this trend toward tight apical constriction. Anterior apices (1.2) and posterior apices (1.1) had slightly increased in AP:DV ratio (Fig. 3S and V), as was the case in controls, but unlike controls, anterior (60 μm^2) and posterior (41 μm^2) apices had expanded considerably (Fig. 3S, W, $p < 0.001$). By late S12, anterior apices (72 μm^2) and posterior apices (40 μm^2) had slowed their expansion and now exhibited surface areas similar to controls (Fig. 3T, W), but overall, this expansion had occurred without any AP bias; neither anterior nor posterior apices had increased in AP:DV ratio (S12E = 1.2, S12L = 1.3), and both were significantly lower than controls ($p < 0.001$). These results revealed a failure of AP-biased expansion in *brL > shi[K44A]* roof FCs (Fig. 3T, V). By S13, the behavior of anterior apices had diverged from that of posterior apices, and neither resembled controls. Surprisingly, anterior apices had expanded to 159 μm^2, and posterior apices had expanded to 91 μm^2; both values were significantly greater than controls (Fig. 3U, W, $p < 0.001$). The AP:DV ratio of anterior vs. posterior apices was 1.4 vs. 1.5, respectively (Fig. 3U, V), again representing a significant departure from controls ($p < 0.001$), and only a slight AP-biased apical expansion.

In summary, control roof FCs constricted their apices during tube formation at S11, then expanded these surfaces such that cells elongated preferentially on the AP axis during S12—S14. In contrast, disruption of Dynamin function in roof FCs caused cells to constrict their apices to an even greater degree than controls, and then expand these surfaces beyond controls in all directions, with little or no directional bias to the expansion, and without extending the DA tube in an anterior direction.

3.5. Dynamin's function in DA tubulogenesis is to promote endocytosis

Other studies have shown that Dynamin's functions include but are not limited to endocytosis (e.g., Sever et al., 2013; Thompson et al., 2004; Soulet et al., 2006). Therefore, we sought to determine whether Dynamin's function in DA tubulogenesis is to facilitate endocytosis. We

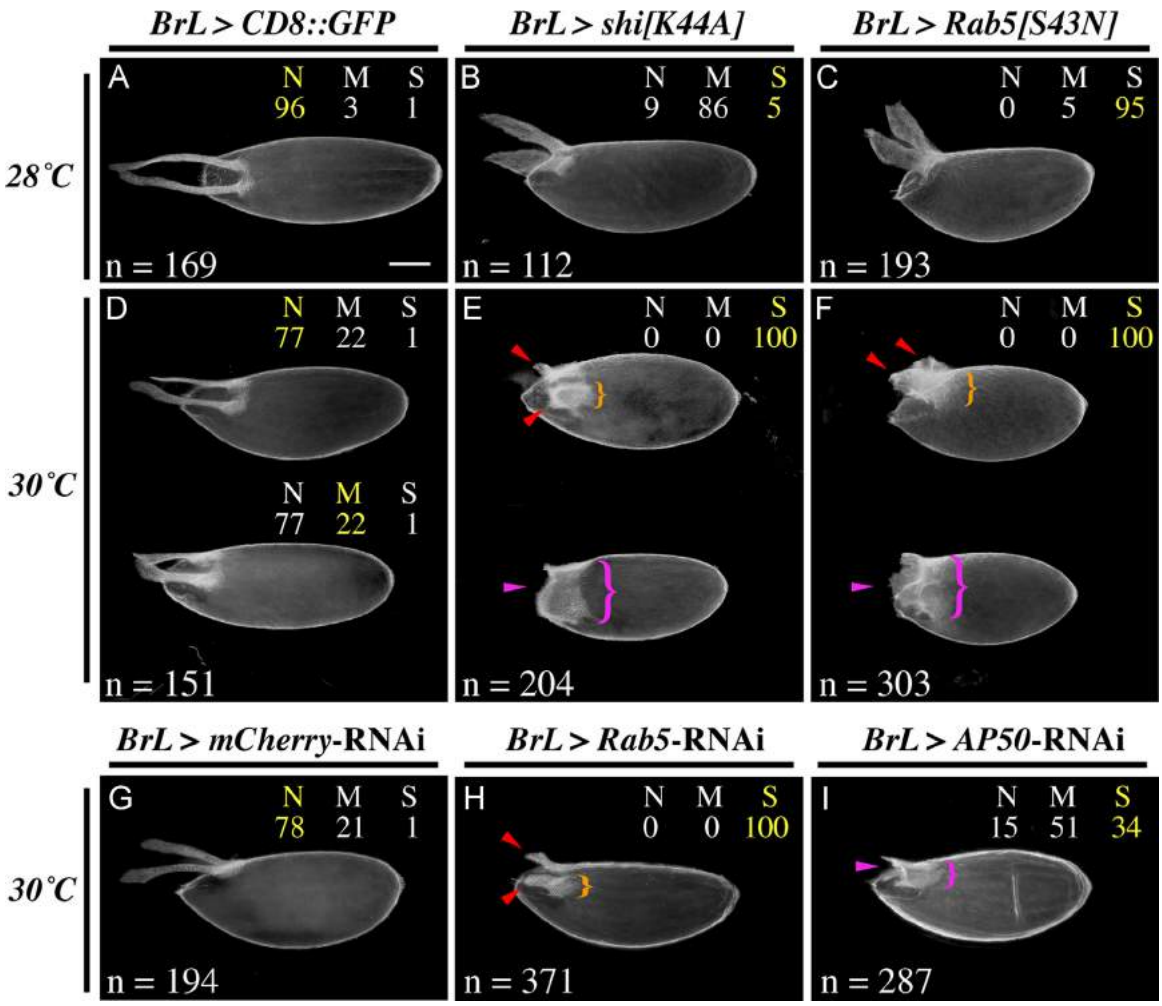

Fig. 4. Defects associated with DA-tube-cell expression of dominant-negative Dynamin are consistent with a disruption of endocytosis. (A–F) Laid eggs from control *brL > CD8::GFP* (A, D), *brL > shi[K44A]* (B, E), or *brL > Rab5[S43N]* (C, F) females, raised at either 28 °C (A–C) or 30 °C (D–F). (G–I) Laid eggs from control *brL > mCherry*-RNAi (G), *brL > Rab5*-RNAi (H), or *brL > AP50*-RNAi (I) females, raised at 30 °C. Numbers indicate percentages of normal or mildly defective (N), moderately defective (M), and severely defective (S) DAs; yellow numbers indicate the category of egg being shown. The number of eggs scored for each condition is shown in the lower left of each panel. Red arrowheads indicate abnormally wide DAs, orange brackets indicate abnormally wide DA bases, purple arrowheads indicate DA fusions, and purple brackets indicate fused DA bases. Scale bar = 100 μm.

disrupted the function of two other well-characterized endocytic players, Rab5 and AP50, and compared their eggshell phenotypes to those of *brL > shi[K44A]* (Fig. 4; these data are distinct from the data in Fig. 1). The Rab5 GTPase is a rate-limiting component of the early endocytic pathway (Bucci et al., 1992), and mutant Rab5[S34N] protein (S43N in *D. melanogaster*) acts as a strong dominant negative (Stenmark et al., 1994). At 28 °C, the *brL > Rab5[S43N]* eggs exhibited a high frequency of severe DA defects (short, broad DAs) compared to controls (Fig. 4A and C); *brL > shi[K44A]* eggs were similar in phenotype, although the frequency of severe defects was much lower (Fig. 4B). At 30 °C, the frequency and severity of DA defects on *brL > shi[K44A]* and *brL > Rab5[S43N]* eggs were indistinguishable: DA fusions were frequent (Fig. 4E and F), and eggshells displayed a similar shortened length compared with controls (Fig. 4D, E, and F). In addition, loss of function through expression of *Rab5*-RNAi resulted in a severe and fully penetrant stunted DA phenotype compared to controls (compare Fig. 4G and H). The stunted DAs of *brL > Rab5*-RNAi eggs were less broad than those of *brL > Rab5[S43N]* eggs, suggesting that *Rab5*-RNAi expression was weaker and/or less able to produce an effect due to perdurance of Rab5 protein compared to expression of dominant-negative Rab5[S43N] (compare Fig. 4F and H).

The AP2-adaptor complex is the primary membrane adaptor for clathrin, and RNAi against AP50 (AP2 subunit μ) is an effective tool for disrupting AP2 function and clathrin-mediated endocytosis (Motley et al., 2003; Boucrot et al., 2010, McMahon and Boucrot, 2011). The DAs of *brL > AP50*-RNAi eggs were wide, had irregular edges, and were sometimes fused (Fig. 4I), supporting the hypothesis that clathrin-mediated endocytosis facilitates DA-tube morphogenesis. These defects were not as severe or penetrant as those produced by *Rab5*-RNAi, Rab5[S43N], or shi[K44A], perhaps reflecting an incomplete knockdown of AP50, which can be difficult to fully deplete (Boucrot et al., 2010). Taken together, these results support a role for Dynamin in facilitating clathrin-mediated endocytosis and demonstrate a requirement for endocytosis during DA tubulogenesis.

3.6. Dynamin is present both apically and basally in DA-tube cells

To identify potential targets of Dynamin-mediated endocytosis within DA-tube FCs, we examined the localization of endogenous Dynamin protein during normal DA tubulogenesis (Fig S2). We observed the highest levels of Dynamin protein in the stretch FCs, consistent with previous mRNA expression data (Peters et al., 2013), and this expression increased over the course of DA tubulogenesis (Fig. S2A–D). In DA-tube FCs, Dynamin protein redistributed from lateral membranes to the cytoplasm between S10B—

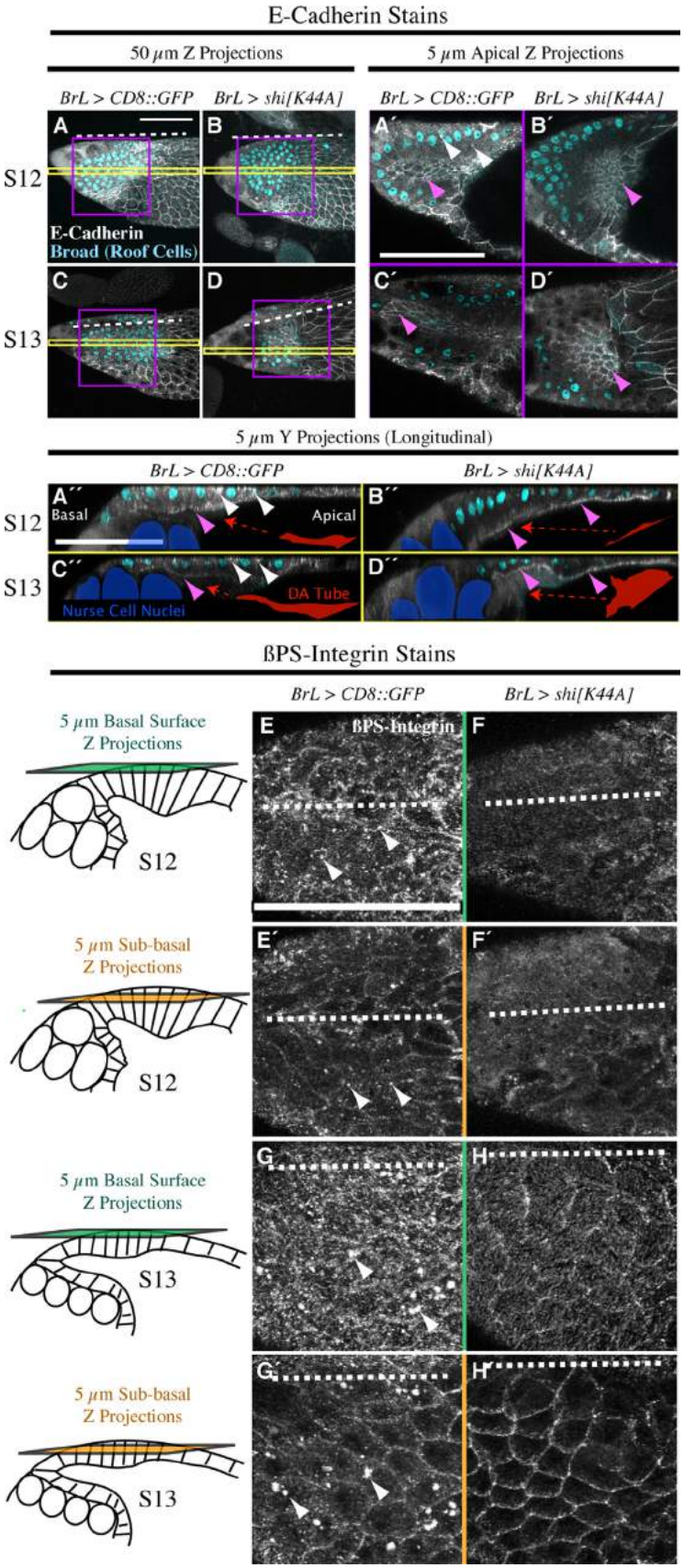

Fig. 5. Expression of dominant-negative Dynamin in DA-tube cells alters E-Cadherin and βPS-Integrin localization. (A–D") Control *brL > CD8::GFP* (A, C, A', C', A", C") vs. *brL > shi[K44A]* (B, D, B', D', B", D") egg chambers, stained for Broad protein (roof cell nuclei) and E-Cadherin. (A–D) 50-μm *Z* projections are shown for staging and to orient the images shown in A'–D' and A"–D". (A'–D') 5-μm apical Z projections (corresponding to purple boxes in A–D) show top-down views of the apices of roof cells. (A"–D") 5-μm longitudinal Y projections (corresponding to yellow boxes in A–D) show the shape of the DA tube (red shapes and red arrows), the distribution of roof cell nuclei (cyan), the position of the DA tube relative to the nurse cell nuclei (blue), and the distribution of E-Cadherin along the apical-basal axis of the roof cells. White arrowheads indicate cytoplasmic puncta of E-Cadherin, and pink arrowheads indicate apical E-Cadherin. (E–H') Control *brL > CD8::GFP* (E, E', G, G') vs. *brL > shi[K44A]* (F, F', H, H') egg chambers, stained for ßPS-Integrin. Schematics to the left indicate the approximate location along the apical-basal axis of the *Z* projections to the right. Green panels represent 5-μm Z projections of the basal surface, and orange panels represent 5-μm Z projections just apical to the basal surface. Dotted lines indicate dorsal midlines, and white arrowheads indicate puncta of ßPS-Integrin. Scale bars = 100 μm.

S12 relative to adjacent main body FCs (Fig. S2A and D), and by S12, the difference between DA-tube-FC Dynamin and main-body-FC Dynamin was distinct (Fig. S2D). Subcellular inspection of DA-tube FCs indicated that Dynamin protein was most prominent at cell apices (Fig. S2E) and on the basal surface (Fig. S2F). We also observed unexpected nuclear Dynamin signal, but we reasoned that this apparent sub-cellular distribution was likely due to cross-reactivity of the Dynamin antibody, which was polyclonal and unpurified. To obtain an independent evaluation of Dynamin localization, we drove expression of Dynamin::YFP (*UASp-shi::YFP*; Fabrowski et al., 2013) using the *Vm26Aa-GAL4* driver; *Vm26Aa-GAL4* expresses in all columnar FCs, but because the *UASp-shi::YFP* was designed for germline, not somatic, expression, Dyn::YFP-was only visible in some cells. This mosaic expression let us visualize Dynamin::YFP in individual cells (Fig. S2G) and confirmed that the highest concentration of Dynamin was present apically and basally in DA-tube cells (yellow arrowheads), in contrast to nearby midline cells (pink arrowhead) or main body FCs (data not shown). Furthermore, the absence of nuclear Dyn::YFP indicated that the Dynamin antibody did recognize a non-specific target(s) (Fig. S2G). To verify that the Dynamin antibody actually recognized Dynamin, we stained *Vm26Aa > shi::YFP* egg chambers for Dynamin; we observed co-localization of Dynamin antibody with Dyn::YFP (Fig. S2H). Together, these observations suggested that Dynamin might be functioning both apically and basally to promote DA tubulogenesis.

3.7. Disruption of Dynamin function alters E-Cadherin and Integrin localization

We hypothesized that apically localized Dynamin could be required for remodeling apical, E-Cadherin-based, cell–cell adhesions, a critical step for morphogenetic events involving cell intercalation and convergent extension (Ulrich et al., 2005; Langevin et al., 2005; Pirraglia et al., 2006, Nishimura and Takeichi, 2009). Therefore, we compared E-Cadherin localization in *brL > CD8::GFP* control and *brL > shi[K44A]* egg chambers at S12, early in DA-tube expansion, and at S13, late in DA-tube expansion (Fig. 5). We used 50 μm Z projections for orientation (Fig. 5A–D), 5 μm apical Z projections to visualize the DA tubes (Fig. 5A'–D'), and 5 μm longitudinal Y Projections to visualize DA-tube cells in profile (Fig. 5A"–D"). In S12 controls, E-Cadherin was present both apically and throughout the cytoplasm (Fig. 5A', A"), whereas in *brL > shi[K44A]* egg chambers, E-Cadherin was primarily apical and relatively absent from the cytoplasm (Fig. 5B' and B"). In S13 controls, as DA-tube elongation progressed, levels of E-Cadherin at the apical domain appeared to decrease, as did the amount of E-Cadherin throughout the cytoplasm (Fig. 5C', C"), but the distribution remained punctate (Fig. 5A" and C", arrowheads). In contrast, *brL > shi[K44A]* egg chambers exhibited an increase in apical E-Cadherin, which was also more evenly distributed, and nearly all cytoplasmic, punctate localization was lost (Fig. 5D' and D"). Consistent with *brL > shi[K44A]* expressing in FC types adjacent to the DA-tube cells, we also observed apical E-Cadherin stabilization and a decrease in cytoplasmic E-Cadherin in FCs posterior and ventral to DA-tube cells (compare Fig. 5A to B and C to D). In summary, *brL > shi[K44A]* egg chambers displayed reduced cytoplasmic E-Cadherin localization compared to controls, more uniform, apical, membrane-associated E-Cadherin than in controls, and these effects became more pronounced with time. These data demonstrate that disrupting Dynamin function alters E-Cadherin localization in FCs, particularly DA-tube cells, and are consistent with Dynamin functioning to remodel apical, E-Cadherin-based adhesions during DA tubulogenesis.

Conversely, we reasoned that basally localized Dynamin could be required for endocytic turnover of basal, Integrin-based adhesions, a critical step for morphogenetic events involving cell migration and tissue elongation (He et al., 2010; Dong et al., 2011; Huttenlocher and Horwitz, 2011; Bogdanovic et al., 2012; Rodriguez-Fraticelli and Martin-Belmonte, 2014). Therefore, we compared the localization of βPS-Integrin (encoded by *myospheroid*) in *brL > CD8::GFP* control and *brL > shi[K44A]* egg chambers during DA-tube elongation (S12—S13; Fig. 5). In DA-tube cells of control egg chambers, βPS-Integrin was present on the basal surface and in basal puncta (Fig. 5E and G), and sub-basally on lateral membranes and in large, cytoplasmic puncta (Fig. 5E' and G'). In DA-tube cells of *brL > shi[K44A]* egg chambers, we observed βPS-Integrin on the basal surface as in controls, but the pattern appeared more diffuse, basal puncta were less conspicuous, and cell outlines were more prominent than controls (compare Fig. 5E to F, G to H). Sub-basally, βPS-Integrin progressively built up on lateral membranes, and the large, cytoplasmic puncta observed in controls were not visible (compare Fig. 5E' to F', G' to H'). In summary, S12 and S13 *brL > shi*[K44A] egg chambers displayed more-ordered basal βPS-Integrin, more-uniform sub-basal βPS-Integrin on lateral membranes, and less-punctate basal and cytoplasmic βPS-Integrin than controls, and these effects increased with time. These data demonstrate that disrupting Dynamin function alters βPS-Integrin localization in DA-tube FCs and are consistent with Dynamin functioning in the turnover of basal, Integrin-based adhesions during DA-tube migration and elongation.

3.8. Altering the behavior of Cadherin- and Integrin-based adhesions demonstrates that the regulation of adhesion molecules is essential for DA tubulogenesis

Disrupting Dynamin function alters the level and sub-cellular distribution of E-Cadherin (Fig. 5, Movies S3 and S4) and βPS-Integrin (Fig. 5), particularly during DA-tube expansion, suggesting that the regulation of both apical and basal adhesive turnover could be an important function of Dynamin. Thus, individually disrupting E-Cadherin- and βPS-Integrin-based adhesions could reveal their separate contributions to DA-tube expansion. To this end, we used *brL-GAL4* to drive the expression of loss-of-function and over-expression constructs and compared the resulting eggshell DA defects to controls (Fig. 6).

First, we assessed the effects of adhesion-component knockdown. DAs of *brL > E-Cadherin*-RNAi eggs were dramatically reduced in length and were located further back on the egg relative to controls (Fig. 6A and B). DAs and DA bases were wider than controls and exhibited both detached chorion particles (white arrow in Fig. 6B) and gaps in eggshell deposition (posterior region of DAs in right egg, Fig. 6B), consistent with loss of cell–cell adhesion and aberrant eggshell secretion. Despite these defects, we did not observe an increased frequency of DA-fusion in *brL > E-Cadherin*-RNAi eggs relative to controls. Knockdown of *β-Integrin-ν*, an Integrin subunit that is primarily expressed in the larval and adult digestive system (Yee and Hynes, 1993), resulted in only modest defects, such as thinner DAs (Fig. 6C), whereas knockdown of *βPS-Integrin (myospheroid)*, the most commonly expressed *Drosophila* β-Integrin, resulted in dramatically stunted DAs that had a kinked shape reminiscent of DAs with distinct stalks and paddles (left egg in Fig. 6D). Occasionally (~5%), these DAs were fused (right egg in Fig. 6D). These results demonstrate that E-Cadherin and βPS-Integrin are both required for DA-tube elongation, but E-Cadherin is important for maintaining DA-tube integrity and uniform eggshell secretion, whereas βPS-Integrin is important for migration and could help maintain DA-tube separation.

To test whether precise levels of E-Cadherin and Integrin expression are important for DA tubulogenesis, we assessed the effects of over-expression. Over-expression of E-Cadherin produced

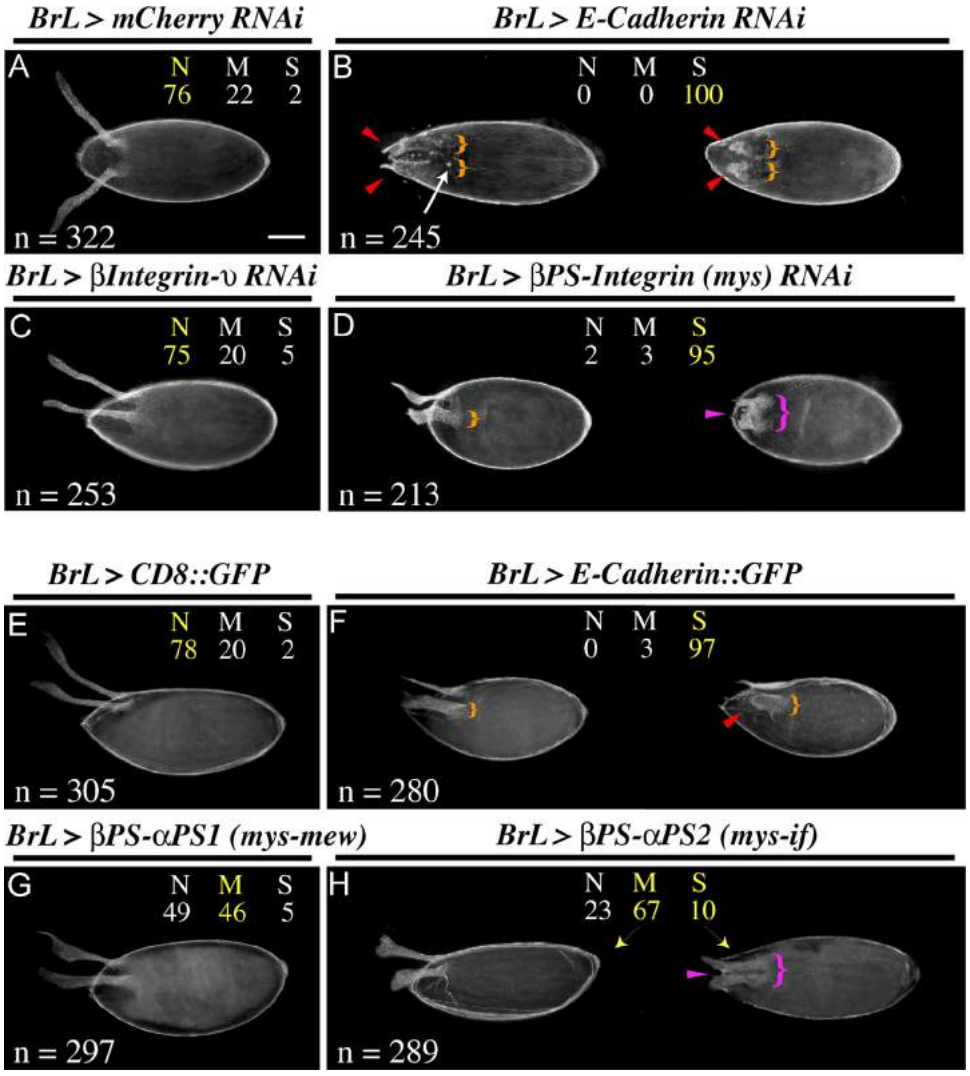

Fig. 6. Regulation of E-Cadherin and Integrin levels are required for DA tubulogenesis. (A–H) Laid eggs from control *brL > mCherry*-RNAi (A), *brL > E-Cadherin* RNAi (B), *brL > β-Integrin-ν* RNAi (C), *brL > βPS-Integrin* RNAi (D), *brL > CD8::GFP* (E), *brL > E-Cadherin::GFP* (F), *brL > βPS-Integrin*, PS1-Integrin (G), and *brL > βPS-Integrin*, PS2-Integrin (H) females, raised at 30 °C. Numbers indicate percentages of normal or mildly defective (N), moderately defective (M), and severely defective (S) DAs; yellow numbers indicate the category of egg being shown. The number of eggs scored for each condition is shown in the lower left of each panel. Red arrowheads indicate abnormally wide DAs, orange brackets indicate abnormally wide DA bases, purple arrowheads indicate DA fusions, and purple brackets indicate fused DA bases. In panel B, note that small globs of DA-eggshell material have become detached from the primary eggshell (white arrow). Scale bar = 100 μm.

some defects similar to E-Cadherin knockdown: DAs of *brL > E-Cadherin::GFP* eggs were short and wide, distinctly formed (i.e., not fused), and placed more posteriorly on the eggshell. The integrity of the DA-tubes was not grossly affected, however, as we observed relatively smooth DA-edges, uniform eggshell secretion, and no notable increase in DA-fusions (Fig. 6E and F). On the other hand, DAs of *brL > βPS-Integrin—αPS1-Integrin* and *brL > βPS-Integrin—αPS2-Integrin* eggs were distinctly different from those of *brL > E-Cadherin::GFP* eggs: DA borders were less roughened, DA paddles were wide and more prominent, and DA bases were occasionally fused (Fig. 6G and H). Interestingly, DA defects were significantly more severe and penetrant with the βPS-Integrin—αPS2-Integrin combination (Fig. 6H), suggesting that these complexes could be the more important Integrin-subunit combination for DA tubulogenesis. Taken together, these results demonstrate that precise regulation of E-Cadherin and Integrin levels is important for DA tubulogenesis, and that altering the behavior of E-Cadherin- and Integrin-based adhesions causes distinct tubulogenic defects.

4. Discussion

Since its discovery and characterization as an essential regulator of clathrin-mediated endocytosis, Dynamin has been indispensably linked to a myriad of cellular processes, particularly those involving membrane remodeling and cytoskeletal regulation (Furguson and De Camilli, 2012). As this study demonstrates, Dynamin-mediated endocytosis can be a major driving force in tissue morphogenesis. Here we identify novel functions for Dynamin in DA-tube closure and DA-tube elongation, and we demonstrate that these functions influence DA-tube length, shape, and position on the eggshell. We show that Dynamin is required within DA-tube cells, and we find that Dynamin serves to facilitate endocytosis in this context. Importantly, within the DA-tube cells, Dynamin function appears to be most important in the roof cells, where it both influences the ability of the floor cells to close the DA-tube and facilitates cell intercalation and biased apical expansion. Our data support a model in which DA-tube formation, cell intercalation, and directionally biased apical expansion are required for DA-

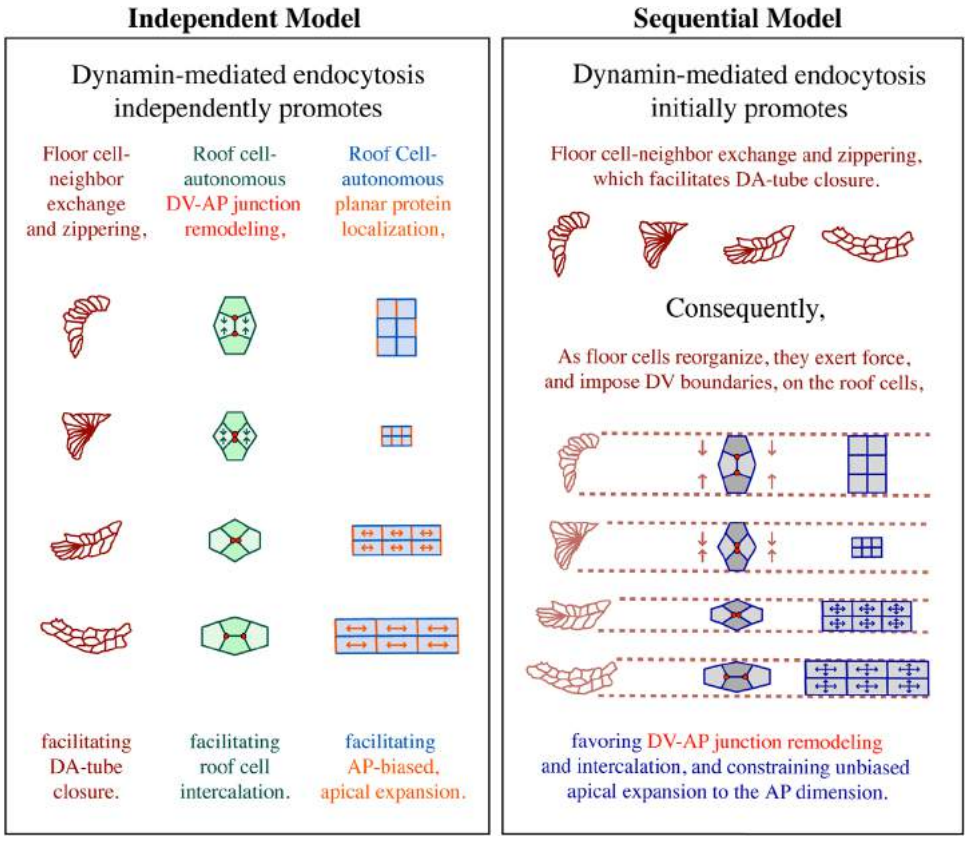

Fig. 7. Models for the relationship of the DA-tubulogenic cell movements regulated by Dynamin. Dynamin is required for closure of the tube by floor cells during DA-tube formation as well as roof–cell intercalation and biased apical expansion during DA-tube elongation. In the independent model, Dynamin facilitates each of these events separately, and the events corresponding to DA-tube elongation are autonomous to the roof cells and do not depend on DA-tube formation. In the sequential model, the closure of the DA-tube by the floor cells during DA-tube formation imposes spatial boundaries on the subsequent steps of DA-tube expansion so that roof–cell intercalation and biased apical expansion rely on successful DA-tube formation. Dotted lines represent DV boundaries imposed by floor cells on the overlying roof cells, red circles represent cell–cell junctions, orange represents proteins with planar localization, and arrows represent autonomous forces, if located within a cell, or external forces, if located outside a cell.

tube elongation, and we propose that Dynamin promotes these processes through the spatial and temporal modulation of cellular adhesions. Based on these findings, we describe two potential tissue-level mechanisms for how Dynamin regulates tube formation and tube elongation (Fig. 7).

4.1. Towards a complete understanding of tube cell behavior during DA tubulogenesis

DA tubulogenesis is an elegant system for understanding how cell shape-change, adhesion, and migration contribute to epithelial tubulogenesis, without the complications presented by cell division and apoptosis (Dorman et al., 2004; Berg 2005; Osterfield et al., 2013). Recently, Osterfield and colleagues characterized the behavior of floor cells during DA-tube formation in precise detail, and they developed a mathematical model demonstrating that a pattern of line tensions along apical floor cell edges is sufficient to drive tube formation (Osterfield et al., 2013). Although this model offers an elegant and plausible explanation for cell behaviors during DA-tube formation, our data suggest that the roof cells also make an important contribution to, and are indeed essential for, DA-tube formation. In the roof cells, Dynamin-mediated endocytosis could serve to disengage cell–cell adhesions between roof and floor cells, giving the floor cells the motility they need to seal off the DA tube. Thus, DA-tube formation may require both Dynamin-mediated neighbor exchanges between roof and floor cells, as well as floor-cell-autonomous tension and movement.

In addition to identifying a requirement for Dynamin in DA-tube formation, we provide a precise analysis of DA-tube elongation, documenting the spatially and temporally regulated intercalation of roof FCs and biased expansion of roof-FC luminal apices. We demonstrate that between S12—S14, roof FCs intercalate such that each primordium experiences an ~3-fold reduction in DV width and an ~3-fold extension in AP length, and this roof-FC intercalation is accompanied by a rapid expansion of luminal apices with a nearly 3-fold anterior to lateral bias. Additionally, we highlight temporal and terminal differences in apical surface-area regulation of anterior roof FCs, which secrete the wider DA paddles, with respect to posterior roof FCs, which secrete the narrower DA stalks. We propose that these directed intercalation and apical expansion behaviors in roof FCs are necessary for DA-tube elongation, since in their absence, DA tubes are uniformly short and wide. To complete this picture of DA-tube elongation, a precise, quantified characterization of floor-FC behavior during DA-tube elongation will be required, for it is clear that the floor FCs are essential for interactions between migrating DA-tube cells and their stretch FC substrate, and for the proper shaping of the DA tubes (Tran and Berg 2003; Dorman et al., 2004; Boyle et al., 2010).

4.2. Distinct cellular movements of DA tubulogenesis require the GTPase activity of Dynamin

Analyses of eggshell and DA-tube-cell morphology resulting from FC-expression of GTPase-defective Dynamin[DN] indicate that Dynamin's GTPase activity is required for distinct cellular movements of both DA-tube formation and elongation. Notably, Dynamin's function is not just one of general FC maintenance, as

Dynamin[DN]-expressing egg chambers complete oogenesis and secrete eggshell proteins on a similar timescale to controls. Though this Dynamin[DN] may not behave exactly like a *dynamin* null, and non-GTPase-dependent Dynamin functions could also affect DA tubulogenesis, the defects we observe are strong, penetrant, specific, and informative.

What are these distinct cellular movements facilitated by Dynamin, and how might they be related to one another? Initially, Dynamin promotes closure of the DA-tube by the floor cells during DA-tube formation, as demonstrated by the invariant failure of DA-tube closure following Dynamin[DN] expression. Subsequently, Dynamin fosters roof–cell intercalation and biased apical expansion during DA-tube elongation; disrupting these processes with Dynamin[DN] expression produces short, wide DAs. We propose that these cellular movements could either be entirely independent of one another (Fig. 7; independent model) or that the movements of DA-tube elongation could be impacted by the success of tube closure during DA-tube formation (Fig. 7; sequential model). If the movements are independent, then we propose Dynamin promotes roof–cell intercalation through autonomous junctional exchange and biased apical expansion through polarized localization of apical expansion machinery (Fig. 7; independent model). If the movements of DA-tube elongation rely, in whole or in part, on DA-tube closure, then we propose that spatial boundaries imposed by the floor cells could drive, or at least contribute to, tube–cell junctional exchange and intercalation; floor-cell-shape constraints could also restrict generalized roof–cell apical expansion to the AP dimension (Fig. 7; sequential model). These hypotheses predict distinct requirements for Dynamin during the temporal progression of DA tubulogenesis.

Understanding the role of Dynamin in each of these processes will require more detailed analysis of fixed tissue, the development of live-imaging tools that can distinguish floor cells from overlying roof cells, the identification or production of *GAL4* lines specific to roof cells, the production of expression tools without adverse effects on DA tubulogenesis, the creation of strains that incorporate temporal controls on gene disruption, and the generation of Dynamin[DN] constructs that could be activated at subcellular locations in living tissue to enable analyses of apical and basal functions.

4.3. Dynamin facilitates DA tubulogenesis through endocytosis

Dynamin's repertoire of cellular functions extends beyond endocytosis and includes many other forms of membrane deformation, regulation of actin and microtubule dynamics, and more (Furgeson and De Camilli, 2012; Sever et al., 2013). However, the similarity of defects we observe following expression of Dynamin [DN], Rab5[DN], *Rab5*-RNAi, and *AP-50*-RNAi, are consistent with Dynamin promoting DA tubulogenesis through clathrin-mediated endocytosis (McMahon and Boucrot, 2011). Since Rab5 has also been linked to non-clathrin-mediated endocytic processes (Hagiwara et al., 2009; Fabrowski et al., 2013; Diaz et al., 2014), and *AP50*-RNAi expression did not produce as severe defects as Dynamin[DN], Rab5[DN], or *Rab5*-RNAi, we must acknowledge the possibility of a non-clathrin-mediated endocytic contribution of Dynamin to DA tubulgoenesis, Nevertheless, our data strongly support a role for Dynamin in promoting DA tubulogenesis via endocytosis, most likely via clathrin-mediated endocytosis.

4.4. DA tubulogenesis requires the spatiotemporal regulation of cellular adhesion

What are the molecular targets of Dynamin-mediated endocytosis during DA tubulogenesis, and what are the relative contributions of apical endocytosis and basal endocytosis?

Given the observed bias towards apical and basal localization of Dynamin protein in cells undergoing DA tubulogenesis, Cadherin- and Integrin-based adhesions were appealing candidates. E-Cadherin recycling is implicated in a variety of morphogenetic processes, including zebrafish gastrulation, salivary-gland morphogenesis in *Drosophila*, and mouse heart-valve morphogenesis, and in many cases, this requirement has been attributed to clathrin-mediated endocytosis (Ulrich et al., 2005; Pirraglia et al., 2006; Tatin et al., 2013; Goldenberg and Harris, 2013). Likewise, Integrin recycling is a well-documented feature of cell migration and morphogenesis. It has been linked to both clathrin-dependent (Nishimura and Kaibuchi, 2007; Chao and Kunz, 2009; Ezratty et al., 2009; Bogdanovic et al., 2012) and calveolin-dependent endocytosis (Shi and Sottile 2008). In the *Drosophila* salivary gland, PS1-Integrin (*mew*) plays a key role in budding morphogenesis (Pirraglia et al., 2013). It is intriguing that PS2-Integrin (*if*) appears to be more important in the DA tube, which forms by wrapping.

Consistent with these findings, and supporting a role for Dynamin in regulating adhesive turnover during DA tubulogenesis, Dynamin[DN] egg chambers exhibited more stable, uniform apical E-Cadherin, more ordered, basal βPS-Integrin, decreased cytoplasmic localization of these proteins, and a temporal progressivity to these effects. Our evidence suggests that remodeling of cellular adhesions is required for the cell movements of DA tubulogenesis, as individually altering E-Cadherin and Integrin levels, via both RNAi and overexpression, have dramatic and distinct effects on DA tubulogenesis. Indeed, regulating the balance of cellular adhesion appears to be at the very heart of DA tubulogenesis.

In summary, Dynamin likely functions both apically and basally to regulate the remodeling of cellular adhesions during the cell movements of DA tubulogenesis. Thus, loss of Dynamin's GTPase activity disrupts the neighbor exchange that facilitates tube closure and the planar-polarized apical expansion and intercalation that accompany, and likely drive, DA-tube elongation (Fig. 7). Dynamin plays a central role throughout this process of epithelial tube morphogenesis, and we are only beginning to understand the capability and responsibility of this fascinating molecule.

Acknowledgments

We acknowledge Greg Martin at the UW W. M. Keck Microscopy Center for imaging assistance and NIH S10 OD016240 for funding this facility. We thank Kamsi Odinammadu for performing *br[69B08]-GAL4* and other *GAL4* experiments; Stanislav Shvartsman, Anne Sustar, Miriam Osterfield, Mani Ramaswami, Stefano De Renzis, Leo Pallanck, David Bilder, Sally Horne-Badovinac, Steven Hou, Kendal Broadie, Gabrielle Boulianne, the Bloomington Stock Center, the Developmental Studies Hybridoma Bank, and the Vienna Drosophila Resource Center for fly strains and/or reagents; Barbara Wakimoto, Dave Raible, Sandra Zimmerman and Anne Sustar for critical reading of this manuscript; and University of Washington Provost Bridge Funds, NIH 2R01 GM079433, and NSF Graduate Research Fellowship DGE-0718124 for support.

Appendix A. Supplementary material

Supplementary data associated with this article can be found in the online version at http://dx.doi.org/10.1016/j.ydbio.2015.10.034.

References

Andreu, M.J., González-Pérez, E., Ajuria, L., Samper, N., González-Crespo, S., Campuzano, S., Jiménez, G., 2012. Mirror represses *pipe* expression in follicle cells to initiate dorsoventral axis formation in *Drosophila*. Development 139, 1110–1114.

Andrew, D.J., Ewald, A.J., 2010. Morphogenesis of epithelial tubes: Insights into tube formation, elongation, and elaboration. Dev. Biol. 341, 34–55.
Berg, C.A., 2005. The *Drosophila* shell game: patterning genes and morphological change. Trends Genet. 21, 346–355.
Beumer, K.J., Rohrbough, J., Prokop, A., Broadie, K., 1999. A role for PS integrins in morphological growth and synaptic function at the postembryonic neuromuscular junction of *Drosophila*. Development 126, 5833–5846.
Beumer, K.J., Matthies, H.J., Bradshaw, A., Broadie, K., 2002. Integrins regulate DLG/FAS2 via a CaM kinase II-dependent pathway to mediate synapse elaboration and stabilization during postembryonic development. Development 129, 3381–3391.
Bogdanovic, O., Machin-Delfino, M., Nicolas-Perez, M., Gavilan, M.P., Gago-Rodriguez, I., Fernandez-Minan, A., Lillo, C., Rios, R.M., Wittbrodt, J., Martinez-Morales, J.R., 2012. Numb/Numbl-Opo antagonism controls retinal epithelium morphogenesis by regulating integrin endocytosis. Dev. Cell 23, 782–795.
Bosclair Lachance, J.F., Lomas, M.F., Eleiche, A., Kerr, P.B., Nilson, L.A., 2009. Graded Egfr activity patterns the *Drosophila* eggshell independently of autocrine feedback. Development 136, 2893–2902.
Boucrot, E., Saffarian, S., Zhang, R., Kirchhausen, T., 2010. Roles of AP-2 in Clathrin-mediated endocytosis. Plos One 5, 1–12.
Boyle, M.J., Berg, C.A., 2009. Control in time and space: Tramtrack69 cooperates with Notch and Ecdysone to repress ectopic fate and shape changes during *Drosophila* egg chamber maturation. Development 136, 4187–4197.
Boyle, M.J., French, R.L., Cosand, A.K., Dorman, J.B., Kiehart, D.P., Berg, C.A., 2010. Division of labor: subsets of dorsal-appendage-forming cells control the shape of the entire tube. Dev. Biol. 346, 68–79.
Brand, A.H., Perrimon, N., 1993. Targeted gene expression as a means of altering cell fates and generating dominant phenotypes. Development 118, 401–415.
Brower, D., Wilcox, M., Piovant, M., Smith, R.J., Reger, L.A., 1984. Related cell-surface antigens expressed with positional specificity in *Drosophila* imaginal discs. Proc. Natl. Acad. Sci. 81, 7485–7489.
Bucci, C., Parton, R.G., Mather, I.H., Stunnenberg, H., Simons, K., Hoflack, B., Zerial, M., 1992. The small GTPase Rab5 functions as a regulatory factor in the early endocytic pathway. Cell 70, 715–728.
Chao, W., Kunz, J., 2009. Focal adhesion disassembly requires clathrin-dependent endocytosis of integrins. FEBS Lett. 583, 1337–1343.
Chappie, J.S., Mears, J.A., Fang, S., Leonard, M., Schmid, S.L., Milligan, R.A., Hinshaw, J.E., Dyda, F., 2011. A pseudoatomic model of the dynamin polymer identifies a hydrolysis-dependent power stroke. Cell 147, 209–222.
Chappie, J.S., Dyda, F., 2013. Building a fission machine – structural insights into dynamin assembly and activation. J. Cell Sci. 126, 2773–2784.
Chua, J., Rikhy, R., Lippincott-Schwartz, J., 2009. Dynamin 2 orchestrates the global actomyosin cytoskeleton for epithelial maintenance and apical constriction. Proc. Natl. Acad. Sci. 106, 20770–20775.
Diaz, J., Mendoza, P., Ortiz, R., Diaz, N., Leyton, L., Stupack, D., Quest, A.F.G., Torres, V. A., 2014. Rab5 is required in metastatic cancer cells for Caveolin-1- enhanced Rac1 activation, migration and invasion. J. Cell Biol. 127, 2401–2406.
Dong, B., Deng, W., Jiang, D., 2011. Distinct cytoskeleton populations and extensive crosstalk control *Ciona* notochord tubulogenesis. Development 138, 1631–1641.
Dorman, J.B., James, K.E., Fraser, S.E., Kiehart, D.P., Berg, C.A., 2004. *bullwinkle* is required for epithelial morphogenesis during *Drosophila* oogenesis. Dev. Biol. 267, 320–341.
Dubreuil, R., Byers, T.J., Branton, D., Goldstein, L.S., Kiehart, D.P., 1987. *Drosophila* spectrin I. Characterization of the purified protein. J. Cell Biol. 105, 2095–2102.
Emery, I.F., Bedian, V., Guild, G.M., 1994. Differential expression of Broad-Complex transcription factors may forecast tissue-specific developmental fates during *Drosophila* metamorphosis. Development 120, 3275–3287.
Estes, P.S., Roos, J., van der Bliek, A., Kelly, R.B., Krishnan, K.S., Ramaswami, M., 1996. Traffic of dynamin within individual *Drosophila* synaptic boutons relative to compartment-specific markers. J. Neurosci. 16, 5443–5456.
Ezratty, E.J., Bertaux, C., Marcantionio, E.E., Gunderson, G.G., 2009. Clathrin mediates integrin endocytosis for focal adhesion disassembly in migrating cells. J. Cell Biol. 187, 733–747.
Fabrowski, P., Necakov, A.S., Mumbauer, S., Loeser, E., Reversi, A., Streichan, S., Briggs, J.A.G., De Renzis, S., 2013. Tubular endocytosis drives remodelling of the apical surface during epithelial morphogenesis in *Drosophila*. Nat. Commun. 4, 1–12.
Fuchs, A., Cheung, L.S., Charbonnier, E., Shvartsman, S.Y., Pyrowolakis, G., 2012. Transcriptional interpretation of the EGF receptor signaling gradient. Proc. Natl. Acad. Sci. USA 109, 1572–1577.
Furgeson, S.M., De Camilli, P., 2012. Dynamin, a membrane-remodeling GTPase. Nat. Rev. Mol. Cell. Biol. 13, 75–88.
Goldenberg, G., Harris, T.J.C., 2013. Adherens junction distribution mechanisms during cell-cell contact elongation in *Drosophila*. Plos One 8, 1–14.
Gomez, J.M., Wang, Y., Riechmann, V., 2012. Tao controls epithelial morphogenesis by promoting Fasciclin 2 endocytosis. J. Cell Biol. 199, 1131–1143.
Gray, N.W., Kruchten, A.E., Chen, J., McNiven, M.A., 2005. A dynamin-3 spliced variant modulates the actin/cortactin-dependent morphogenesis of dendritic spines. J. Cell Sci. 118, 1279–1290.
Hagiwara, M., Shirai, Y., Nomura, R., Sasaki, M., Kobayashi, K., Tadokoro, T., Yamamoto, Y., 2009. Caveolin-1 activates Rab5 and enhances endocytosis through direct interaction. Biochem. Biophys. Res. Commun. 378, 73–78.
He, L., Wang, X., Tin, H.A.U., Montell, D.J., 2010. Tissue elongation requires oscillating contractions of a basal actomyosin network. Nat. Cell Biol. 12, 1133–1142.
Huang, J., Zhou, W., Dong, W., Watson, A.M., Hong, Y., 2009. Directed, efficient, and versatile modifications of the *Drosophila* genome by genomic engineering. Proc. Natl. Acad. Sci. 106, 8284–8289.
Huttenlocher, A., Horwitz, A.R., 2011. Integrins in cell migration. Cold Spring Harb. Perspect. Biol. 3, 1–16.
Ip, Y.T., Park, R.E., Kosman, D., Bier, E., Levine, M., 1992. The *dorsal* gradient morphogen regulates stripes of *rhomboid* expression in the presumptive neuroectoderm of the *Drosophila* embryo. Genes Dev. 6, 1728–1739.
Iruela-Arispe, M.L., Beitel, G.J., 2013. Tubulogenesis. Development 140, 2851–2855.
Jenett, A., Rubin, G.M., Ngo, T.-T.B., Shepherd, D., Murphy, C., Dionne, H., Pfeiffer, B. D., et al., 2012. A GAL4-driver line resource for *Drosophila* neurobiology. Cell. Rep. 2, 991–1001.
Langevin, J., Morgan, M.J., Rossé, C., Racine, V., Sibarita, J., Aresta, S., Murthy, M., Schwarz, T., Camonis, J., Bellaiche, Y., 2005. *Drosophila* exocyst components Sec5, Sec6, and Sec15 regulate DE-Cadherin trafficking from recycling endosomes to the plasma membrane. Dev. Cell. 9, 365–376.
Lee, J.Y., Harland, R.M., 2010. Endocytosis is required for efficient apical constriction during *Xenopus* gastrulation. Curr. Biol. 20, 253–258.
Lee, M.Y., Skoura, A., Park, E.J., Landskroner-Eiger, S., Jozsef, L., Luciano, A.K., Murata, T., Pasula, S., Dong, Y., Bouaouina, M., Calderwood, D.A., Ferguson, S.M., De Camilli, P., Sessa, W.C., 2014. Dynamin 2 regulation of integrin endocytosis, but not VEGF signaling, is crucial for developmental angiogenesis. Development 141, 1465–1472.
Lepage, S.E., Bruce, A.E., 2014. Dynamin-dependent maintenance of epithelial integrity is essential for zebrafish epiboly. Bioarchitecture 4, 31–34.
McMahon, H.T., Boucrot, E., 2011. Molecular mechanism and physiological functions of clathrin-mediated endocytosis. Nat. Rev. Mol. Cell. Biol. 12, 517–533.
Moline, M.M., Southern, C., Bejsovec, A., 1999. Directionality of Wingless protein transport influences epidermal patterning in the *Drosophila* embryo. Development 126, 4375–4384.
Motley, A., Bright, N.A., Seaman, M.N.J., Robinson, M.S., 2003. Clathrin-mediated endocytosis in AP-2–depleted cells. J. Cell. Biol. 162, 909–918.
Nishimura, T., Takeichi, M., 2009. Remodeling of the adherens junctions during morphognesis. Curr. Top. Dev. Biol. 89, 33–54.
Nishimura, T., Kaibuchi, K., 2007. Numb controls integrin endocytosis for directional cell migration with aPKC and PAR-3. Dev. Cell 13, 15–28.
Oda, H., Uemura, T., Harada, Y., Iwai, Y., Takeichi, M., 1994. A *Drosophila* homolog of Cadherin associated with Armadillo and essential for embryonic cell–cell adhesion. Dev. Biol. 165, 716–726.
Oda, H., Tsukita, S., 1999. Nonchordate classic cadherins have a structurally and functionally unique domain that is absent from chordate classic cadherins. Dev. Biol. 216, 406–422.
Ogata, S., Morokuma, J., Hayata, T., Kolle, G., Niehrs, C., Ueno, N., Cho, K.W., 2007. TGF-beta signaling-mediated morphogenesis: modulation of cell adhesion via cadherin endocytosis. Genes Dev. 21, 1817–1831.
Osterfield, M., Du, X., Schüpbach, T., Wieschaus, E., Shvartsman, S.Y., 2013. Three-dimensional epithelial morphogenesis in the developing *Drosophila* egg. Dev. Cell 24, 400–410.
Peters, N.C., Thayer, N.H., Kerr, S.A., Tompa, M., Berg, C.A., 2013. Following the 'tracks': Tramtrack69 regulates epithelial tube morphogenesis in the *Drosophila* ovary through Dynamin, Paxillin, and the homeobox protein Mirror. Dev. Biol. 378, 154–169.
Pfeiffer, B.D., Truman, J.W., Rubin, G.M., 2012. Using translational enhancers to increase transgene expression in *Drosophila*. Proc. Natl. Acad. Sci. USA. 109, 6626–6631.
Pirraglia, C., Jattani, R., Myat, M.M., 2006. Rac function in epithelial tube morphogenesis. Dev. Biol. 290, 435–446.
Pirraglia, C., Walters, J., Myat, M.M., 2010. Pak1 control of E-Cadherin endocytosis regulates salivary gland lumen size and shape. Development 137, 4177–4189.
Pirraglia, C., Walters, J., Ahn, N., Myat, M.M., 2013. Rac1 GTPase acts downstream of αPS1βPS integrin to control collective migration and lumen size in the *Drosophila* salivary gland. Dev. Biol. 377, 1–21.
Ray, H.J., Niswander, L., 2012. Mechanisms of tissue fusion during development. Development 139, 1701–1711.
Rodriguez-Fraticelli, A.E., Martin-Belmonte, F., 2014. Picking up the threads: extracellular matrix signals in epithelial morphogenesis. Curr. Opin. Cell. Biol. 30, 83–90.
Schneider, C.A., Rasband, W.S., Eliceiri, K.W., 2012. NIH Image to ImageJ: 25 Years of Image Analysis. Nat. Methods 9; , pp. 671–675.
Sever, S., Chang, J., Gu, C., 2013. Dynamin rings: not just for fission. Traffic 14, 1194–1199.
Shi, F., Sottile, J., 2008. Caveolin-1-dependent β1 integrin endocytosis is a critical regulator of fibronectin turnover. J. Cell. Sci. 121, 2360–2371.
Soulet, F., Schmid, S.L., Damke, H., 2006. Domain requirements for an endocytosis-independent, isoform-specific function of dynamin-2. Exp. Cell Res. 312, 3539–3545.
Stenmark, H., Parton, R.G., Steele-Mortimer, O., Lütcke, A., Gruenberg, J., Zerial, M., 1994. Inhibition of Rab5 GTPase activity stimulates membrane fusion in endocytosis. EMBO J. 13, 1287–1296.
Tatin, F., Taddei, A., Weston, A., Fuchs, E., Devenport, D., Tissir, F., Makinen, T., 2013. Planar cell polarity protein Celsr1 regulates endothelial adherens junctions and directed cell rearrangements during valve morphogenesis. Dev. Cell 26, 31–44.
Thompson, H.M., Cao, H., Chen, J., Euteneur, U., McNiven, M.A., 2004. Dynamin 2 binds γ-tubulin and participates in centrosome cohesion. Nat. Cell Biol. 6, 335–342.
Tran, D.H., Berg, C.A., 2003. Bullwinkle and Shark regulate dorsal-appendage morphogenesis in *Drosophila* oogenesis. Development 130, 6273–6282.
Tzolovsky, G., Deng, W.M., Schlitt, T., Bownes, M., 1999. The function of the *broad-*

complex during *Drosophila melanogaster* oogenesis. Genetics 153, 1371–1383.
Ulrich, F., Krieg, M., Schotz, E., Link, V., Castanon, I., Schnabel, V., Taubenberger, A., Mueller, D., Puech, P., Heisenberg, C., 2005. Wnt11 functions in gastrulation by controlling cell cohesion through Rab5c and E-Cadherin. Dev. Cell 9, 555–564.
van der Bliek, A.M., Meyerowitz, E.M., 1991. Dynamin-like protein encoded by the *Drosophila shibire* gene associated with vesicular traffic. Nature 351, 411–414.
van der Bliek, A.M., Redelmeier, T.E., Damke, H., Tisdale, E.J., Meyerowitz, E.M., Schmid, S.L., 1993. Mutations in human Dynamin block an intermediate stage in coated vesicle formation. J. Cell. Biol. 122, 553–563.
van der Meer, J.M., 1977. Optical clean and permanent whole mount preparation for phase-contrast microscopy of cuticular structures of insect larvae. Drosoph. Inf. Serv. 52, 160.
Wallingford, J.B., 2005. Neural tube closure and neural tube defects: Studies in animal models reveal known knowns and known unknowns. Am. J. Med. Genet. 135C, 59–68.
Ward, E.J., Berg, C.A., 2005. Juxtaposition between two cell types is necessary for dorsal appendage tube formation. Mech. Dev. 122, 241–255.
Yakoby, N., Bristow, C.A., Gong, D., Schafer, X., Lembong, J., Zartman, J.J., Halfon, M. S., Schüpbach, T., Shvartsman, S.Y., 2008. A combinatorial code for pattern formation in *Drosophila* oogenesis. Dev. Cell 15, 725–737.
Yee, G.H., Hynes, R., 1993. A novel tissue-specific integrin subunit βv expressed in the midgut of *Drosophila melanogaster*. Development 118, 845–858.
Zimmerman, S.G., Peters, N.C., Altaras, A.E., Berg, C.A., 2013. Optimized RNA ISH, RNA FISH and protein-RNA double labeling (IF/FISH) in *Drosophila* ovaries. Nat. Protoc. 8, 2158–2179.